

## DIFFUSE X-RAY EMISSION IN A DEEP *Chandra* IMAGE OF THE GALACTIC CENTER

M. P. MUNO,<sup>1,2</sup> F. K. BAGANOFF,<sup>3</sup> M. W. BAUTZ,<sup>3</sup> E. D. FEIGELSON,<sup>4</sup> G. P. GARMIRE,<sup>4</sup> M. R. MORRIS,<sup>1</sup> S. PARK,<sup>4</sup> G. R. RICKER,<sup>3</sup> AND L. K. TOWNSLEY<sup>4</sup>

*To appear in ApJ on 20 September 2004*

### ABSTRACT

We examine the spectrum of diffuse emission detected in the 17' by 17' field around Sgr A\* during 625 ks of *Chandra* observations. The spectrum exhibits He-like and H-like lines from Si, S, Ar, Ca, and Fe, that are consistent with originating in a two-temperature plasma, as well as a prominent low-ionization Fe K- $\alpha$  line. The cooler,  $kT \approx 0.8$  keV plasma differs in surface brightness across the image between  $(0.2 - 1.8) \times 10^{-13}$  erg cm<sup>-2</sup> s<sup>-1</sup> arcmin<sup>-2</sup> (observed, 2–8 keV). This soft plasma is probably heated by supernovae, along with a small contribution from the winds of massive Wolf-Rayet and O stars. The radiative cooling rate of the soft plasma within the inner 20 pc of the Galaxy could be balanced by 1% of the kinetic energy of one supernova every  $3 \times 10^5$  y. The hotter,  $kT \approx 8$  keV component is more spatially uniform, with a surface brightness of  $(1.5 - 2.6) \times 10^{-13}$  erg cm<sup>-2</sup> s<sup>-1</sup> arcmin<sup>-2</sup> (observed; 2–8) keV. The intensity of the hard plasma is correlated with that of the soft, but they are probably only indirectly related, because neither supernova remnants nor WR/O stars are observed to produce thermal plasma hotter than  $kT \approx 3$  keV. Moreover, a  $kT \approx 8$  keV plasma would be too hot to be bound to the Galactic center, and therefore would form a slow wind or fountain of plasma. The energy required to sustain such a freely-expanding plasma within the inner 20 pc of the Galaxy is  $\sim 10^{40}$  erg s<sup>-1</sup>. This corresponds to the entire kinetic energy of one supernova every 3000 y, which is unreasonably high. However, alternative explanations for the  $kT \approx 8$  keV diffuse emission are equally unsatisfying. The hard X-rays are unlikely to result from undetected point sources, because no known population of stellar object is numerous enough to the observed surface brightness. There is also no evidence that non-thermal mechanisms for producing the hard emission are operating, as the expected shifts in the line energies and ratios from their collisional equilibrium values are not observed. We are left to conclude that either there is a significant shortcoming in our understanding of the mechanisms that heat the interstellar medium, or that a population of faint ( $< 10^{31}$  erg s<sup>-1</sup>), hard X-ray sources that are a factor of 10 more numerous than CVs remains to be discovered.

*Subject headings:* acceleration of particles — ISM: structure — Galaxy: center — X-rays: ISM

### 1. INTRODUCTION

Bright, diffuse X-ray and  $\gamma$ -ray emission has been observed all along the Galactic plane, but is particularly bright toward the Galactic center (e.g., Worrall et al. 1982; Koyama et al. 1986b; Yamauchi et al. 1996; Yamasaki et al. 1997; Skibo et al. 1997; Valinia & Marshall 1998). The origin of this emission is uncertain. Unlike the cosmic X-ray background, the Galactic ridge emission has not yet been resolved into discrete point sources. On the one hand, *ASCA* observations revealed degree-scale differences in the surface brightness of the diffuse emission that could only be produced by Poisson fluctuations in the numbers of undetected point sources if they have a luminosity of  $\sim 10^{33}$  erg s<sup>-1</sup> (Yamauchi et al. 1996). On the other hand, *Chandra* observations clearly demonstrate that there are not enough discrete sources with  $L_X \gtrsim 10^{31}$  erg s<sup>-1</sup> to account for more than 10% the Galactic ridge X-ray emission (Ebisawa et al. 2001). However, the strengths of Fe lines observed from the diffuse emission are similar to those observed from Galactic X-ray point sources, which suggests that they could be one and the same (Wang, Gotthelf, & Lang 2002). Furthermore, discrete yet extended sources

could produce the spatial variations in the diffuse emission. Several classes of extended features have recently been identified, including: regions of bright iron fluorescence that are ascribed to molecular clouds being illuminated by X-rays from a bright point source (Sunyaev, Markevitch, & Pavlinsky 1993; Murakami et al. 2000) or bombarded by low-energy cosmic-ray electrons (Yusef-Zadeh, Law, & Wardle 2002); arcminute-scale features with hard spectra that resemble supernova shocks (Bamba et al. 2003); and X-ray counterparts to radio features that are thought to be magnetic filaments (Sakano et al. 2003, Lu, Wang, & Lang 2003). *Chandra* and *XMM-Newton* observations are only beginning to establish how much flux faint point sources and discrete extended features contribute to the diffuse Galactic X-ray emission.

If the Galactic ridge X-ray emission is truly diffuse, then it could be produced either by hot,  $T \gtrsim 10^7$  K plasma or by cosmic-rays interacting with neutral material in the interstellar medium (ISM). The spectrum of the diffuse emission is one of the most useful diagnostics of its origin. *ASCA* observations in the 0.5–10 keV band reveal lines from H-like and He-like ions of Mg, Si, S, and Fe,

<sup>1</sup> Department of Physics and Astronomy, University of California, Los Angeles, CA 90095; mmuno@astro.ucla.edu

<sup>2</sup> Hubble Fellow

<sup>3</sup> Center for Space Research, Massachusetts Institute of Technology, Cambridge, MA 02139

<sup>4</sup> Department of Astronomy and Astrophysics, The Pennsylvania State University, University Park, PA 16802

which indicates that the diffuse emission cannot originate from a plasma with a single temperature (Yamauchi et al. 1996). As a result, several authors have modeled the diffuse emission as originating from two plasma components (e.g., Koyama et al. 1996; Kaneda et al. 1997; Tanaka et al. 2000): one with  $kT_{\text{cool}} \approx 0.8$  keV (which we refer to here as the “cool” or “soft” component), and a second with  $kT_{\text{hot}} \approx 8$  keV (which we refer to as “hot” or “hard”). The soft plasma is thought to be produced by supernova shock-waves (Kaneda et al. 1997), which are the largest source of energy for heating the ISM (Schlickeiser 2002).

The origin of the  $kT \approx 8$  keV component of the Galactic ridge emission is far less certain. The temperature of the putative hot plasma is too high for it to be bound to the Galactic disk, so that the energy required to sustain it could be equivalent to the release of kinetic energy from one supernova occurring every 30 years (e.g., Kaneda et al. 1997; Yamasaki et al. 1997). However, supernovae are not observed to produce thermal plasma with  $kT \gtrsim 3$  keV, and there is no known alternative source in the Galactic disk for that much energy. Therefore, several alternative sources of the hot plasma have been proposed. One possibility is that the  $kT \approx 8$  keV plasma is heated by magnetic reconnection in the ISM, and subsequently confined to the Galactic plane by a large-scale toroidal field (Tanuma et al. 1999). It is also possible that the hot diffuse X-ray emission is a low-energy extension of the emission with a power-law spectrum observed above 10 keV, which suggests that it may result from a non-thermal mechanism (see Skibo et al. 1997; Yamasaki et al. 1997; Valinia & Marshall 1998, but see Lebrun et al. 2004). Among the proposed mechanisms are charge-exchange interactions between cosmic ray ions and interstellar matter (Tanaka, Miyaji, & Hasinger 1999; Valinia 2000), bremsstrahlung radiation from cosmic-ray electrons or protons (Valinia & Marshall 1998), and quasi-thermal emission from plasma that is continuously accelerated by supernova shocks propagating in the  $kT \approx 0.8$  keV component of the ISM (Dogiel et al. 2002; Masai et al. 2002). These non-thermal processes should produce line emission with energies and flux ratios that differ significantly from those expected from a plasma in thermal equilibrium. Unfortunately, previous *ASCA* observations were unable to determine the ionization state of the plasma unambiguously, because the spectrum was contaminated by an instrumental Fe line between 6–7 keV.

Clearly, further study of the diffuse X-ray emission is important for understanding stellar life cycles, magnetic fields, and cosmic ray production in the Galaxy. In this paper, we study the spectral properties of the diffuse X-ray emission from a  $17'$  by  $17'$  field around Sgr A\* that has been observed for over 600 ks with *Chandra*. These observations have several advantages over previous ones with *ASCA* (Koyama et al. 1996) and *BeppoSAX* (Sidoli & Mereghetti 1999): (1) the long integration provides sufficiently large signal-to-noise ratio to study the spectrum of the diffuse emission from arcminute-scale sub-regions of the field, (2) the  $0''.5$  angular resolution allows us to resolve the truly diffuse emission from filamentary features and point sources, and (3) the relative lack of instrumental lines, particularly between 6–7 keV, allows us to measure the ionization state of the diffuse emission with greater

confidence. The layout of the paper is as follows. In Section 2.1 we present images that provide an overview of the diffuse emission from the field. In Section 2.2, we examine how the spectrum of the diffuse emission differs across the field. In Section 2.3, we compare the spectra of the point sources and diffuse emission, and place upper limits on the contribution of undetected point sources to the diffuse emission. In Section 3.1, we derive the properties of the putative plasma responsible for the diffuse emission. These are used in Sections 3.2 and 3.3 to examine the likely origins of the diffuse emission. In Section 3.4, we discuss the number of undetected point sources that may be present in the field. Finally, in Section 4, we list the contributions of point sources, extended features, and diffuse emission to the X-ray luminosity of the Galactic center.

## 2. OBSERVATIONS

The inner 20 pc of the Galaxy have been observed on twelve occasions as of June 2002 (Table 1) using the Advanced CCD Imaging Spectrometer imaging array (ACIS-I) aboard the *Chandra X-ray Observatory* (Weisskopf et al. 2002). The ACIS-I is a set of four 1024-by-1024 pixel CCDs, covering a field of view of  $17'$  by  $17'$ . When placed on-axis at the focal plane of the grazing-incidence X-ray mirrors, the imaging resolution is determined primarily by the pixel size of the CCDs,  $0''.492$ . The CCDs also measure the energies of incident photons, with a resolution of 50–300 eV (depending on photon energy and distance from the read-out node) within a calibrated energy band of 0.5–8 keV.

We reduced the data from each observation using the methods described in detail in Muno et al. (2003a) and Townsley et al. (2003). In brief, we first created an event list for each observation in which we corrected the pulse heights of each event for the position-dependent charge-transfer inefficiency (Townsley et al. 2002a). Next, we excluded events that did not pass the standard *ASCA* grade filters and CXC good-time filters. We then removed intervals in which the count rate from the diffuse emission flared to  $3\text{-}\sigma$  above the mean rate in the 0.5–8.0 keV band, presumably due to particles impacting the detector. This removed all excursions larger than  $\approx 15\%$ , which represented a total time of only 15 ks (2% of the total exposure). The remaining long-term variations in the particle background should be no larger than 5% (see Markevitch et al. 2003). The final total live time was 626 ks.

Before extracting spectra of the diffuse emission, we needed to remove the point sources from the image. To identify the point sources, we created a composite event list by re-projecting the sky coordinates of the events from each observation onto the plane tangent to the radio position of Sgr A\*. We excluded the first half of ObsID 1561 from the composite event list because a bright  $10^{-10}$  erg  $\text{cm}^{-2}$   $\text{s}^{-1}$  transient dominated the northwest portion of the field (GRS 1741.9–2853; see Muno et al. 2003b). An image based upon this event list is displayed in Figure 1. We searched for point sources in images of events in three energy bands (0.5–8 keV, 0.5–1.5 keV, and 4–8 keV) using *wavdetect*. We used a significance threshold of  $10^{-7}$ , which corresponds to the chance of spuriously identifying Poisson fluctuations within a beam defined by the instru-

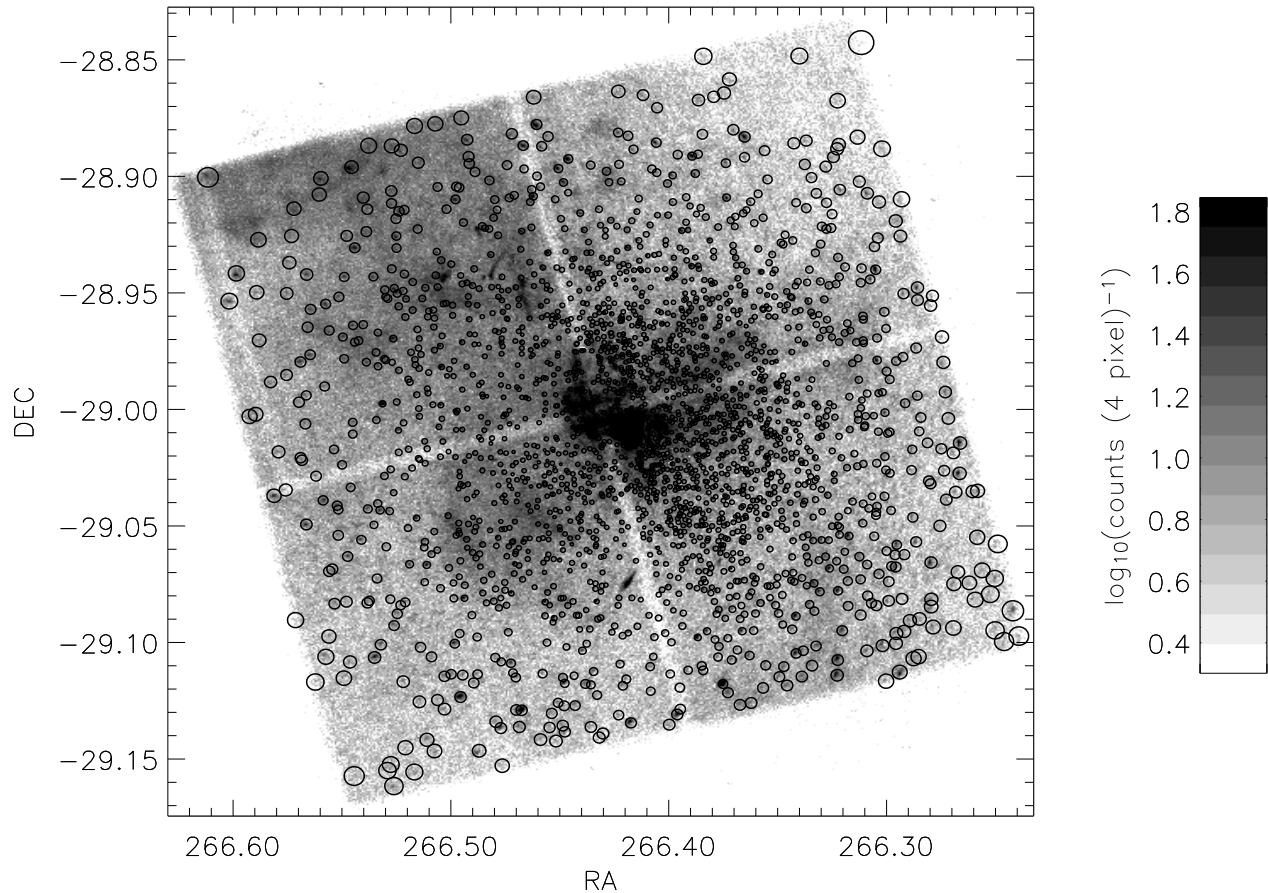


FIG. 1.— Raw image of counts received in the Sgr A\* field. The image has been binned to have  $2''$  pixels. We have overlaid on the image the circles that were used to exclude the 2353 point sources that we detected (Muno et al. 2003a).

mental point spread function (PSF).<sup>5</sup> We identified a total of 2357 X-ray point sources (see Table 3 in Muno et al. 2003a), of which 1792 were detected in the full band, 281 in the soft band (124 exclusively in the soft band), and 1832 in the hard band (441 exclusively in the hard band).

To isolate the diffuse emission in each observation, we excluded events that fell within circles circumscribing the 95% contour of the PSF around each point source. The excluded regions are indicated with circles in Figure 1, and range in size from  $3''$  within  $4'$  of the aim-point to  $7''$  at an offset of  $7.5'$  from the aim-point. We found that the 95% contour struck an appropriate balance between removing most of the counts from point sources in the image, and leaving diffuse emission to analyze. For instance, in the inner few arcminutes of the image, the density of point sources is so high that the circles circumscribing the 99% contour of the PSF cover the image, leaving few counts that are unambiguously diffuse emission. Few photons from the observed point sources should contaminate the diffuse emission. There are only  $2 \times 10^5$  net counts from the point sources in the catalog of Muno et al. (2003a), compared to  $2 \times 10^6$  counts in the diffuse emission, so

fewer than 0.5% of the counts in the diffuse emission should come from the wings of the PSFs for the detected point sources. The flux contributed by the dust-scattering halos of the observed point sources can be estimated using the optical depth toward sources near Sgr A\* from Tan & Draine (2004, their Figures 1 and 8), and the expected energy-dependent profiles of the halos from Draine (2003, their Figures 9 and 10). We estimate that at  $7'$  from the aim-point the scattered component equals the observed point-source flux at 2 keV, but declines to  $\lesssim 20\%$  of the point-source flux above 4 keV. Within  $4'$  of the aim-point the exclusion regions for the point sources are smaller, so the contribution from scattered flux is twice as large. However, point sources produce only 4% of the diffuse flux at 2 keV and 15% above 4 keV (see Section 2.3), so the scattered flux contributes only a few percent to the diffuse emission. For comparison, the systematic uncertainty in the calibration of the CTI-corrected ACIS response is similar, on order 3%.

Finally, we removed the bright, filamentary features identified in the Northeast portion of the image by Park et al. (2004). These features contributed  $\approx 15\%$  of the

<sup>5</sup> We note that this significance was designed to limit the number of spurious sources, and therefore some weak point sources that are difficult to distinguish from statistical fluctuations in the background diffuse emission are not included in the catalog. We ran searches with less strict thresholds, and only identified a couple hundred additional sources. These sources contribute less than 0.5% to the total counts in the diffuse emission, so we let them remain in the image.

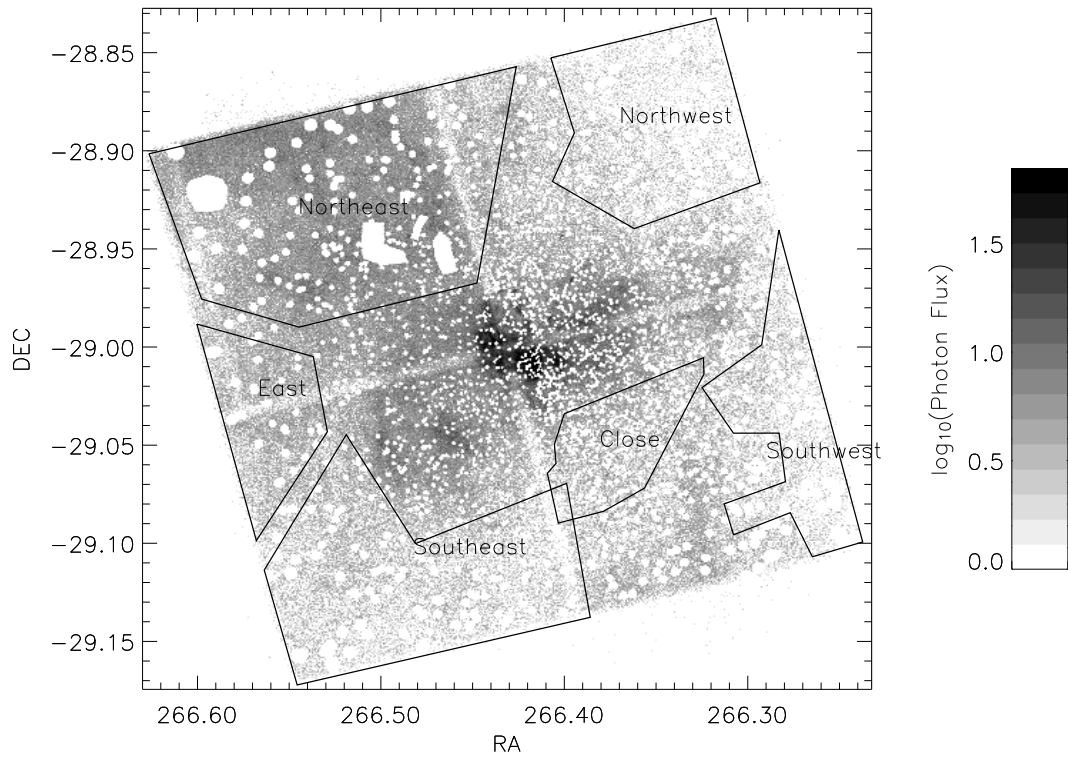


FIG. 2.— Image of the Sgr A\* field in the 2–4 keV band, overlaid with the polygonal regions from which the spectra of the diffuse emission were extracted. The “holes” apparent in the data result from removing events near point sources and obvious filamentary features.

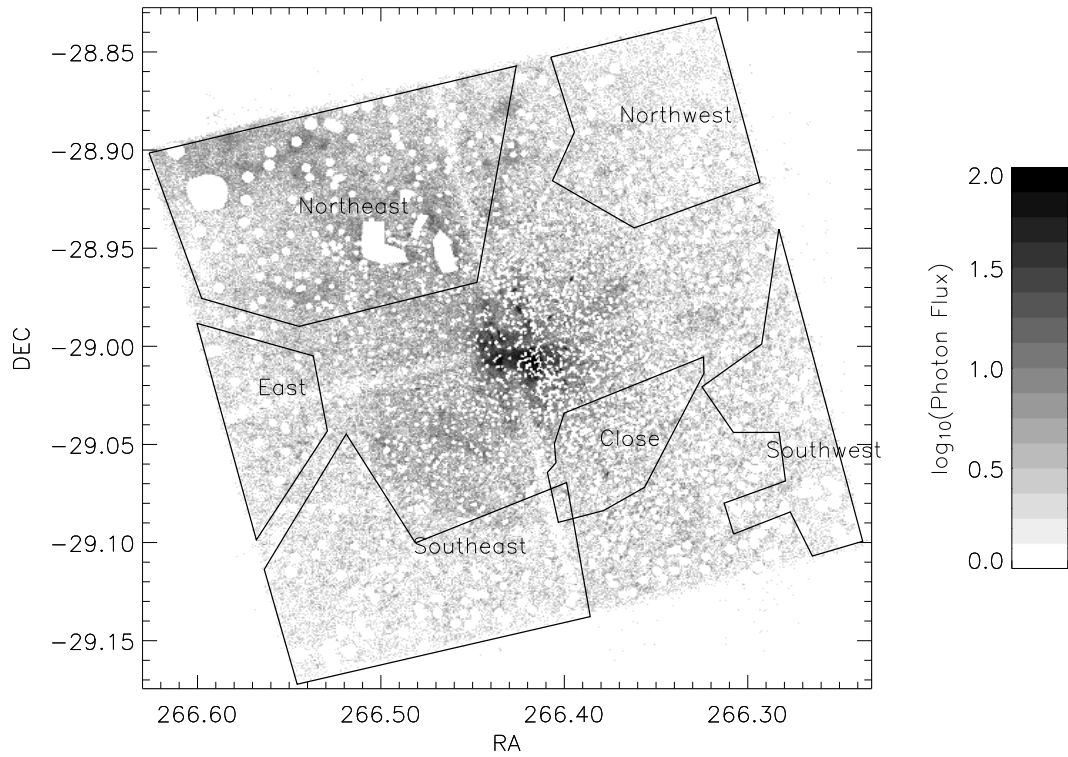


FIG. 3.— Same as Figure 2, for the 4–8 keV band.

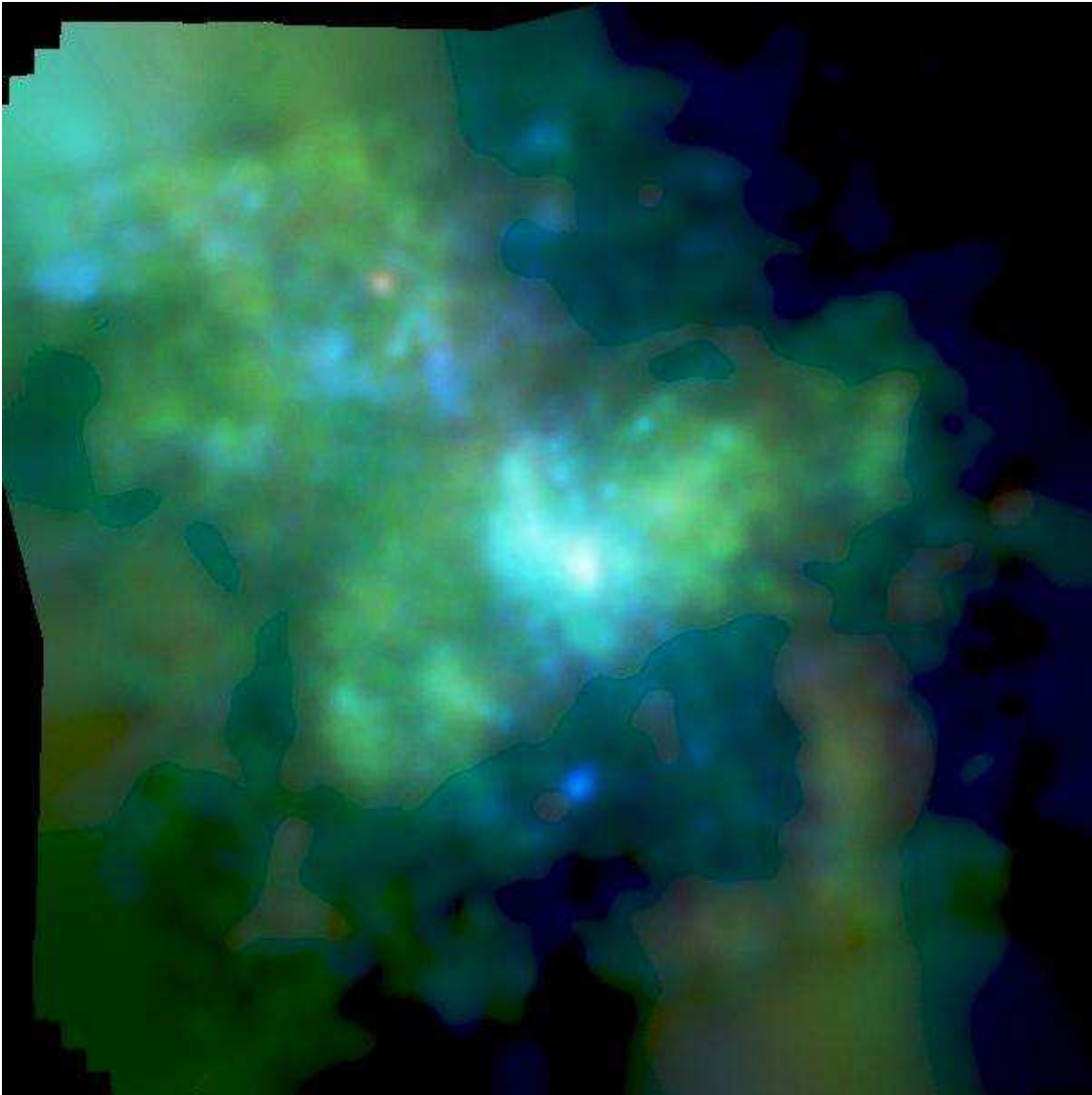


FIG. 4.— Three-color, smoothed image of the Sgr A\* field. The red band is made from photons between 0.5–2.0 keV, the green from 2.0–4.0 keV, and the blue from 4.0–8.0 keV. Point sources were removed from the image as in Figures 2 and 3, and the image was adaptively smoothed using the techniques of Townsley et al. (2003). The intensities of each band were scaled to highlight faint, diffuse features.

flux from this region. We used the resulting event lists to create images and spectra of the diffuse emission.

### 2.1. Images of the Diffuse Emission

We combined the event lists from each observation to produce the images of the diffuse emission in the 2–4 keV and 4–8 keV bands in Figures 2 and 3. The “holes” apparent in the images were left by removing the events associated with the point sources and filamentary features. These images provide a qualitative understanding of the diffuse emission.

In the soft band (2–4 keV), the inner part of the image is dominated by Sgr A\*, the nuclear stellar cluster, and Sgr A East. Beyond these, two lobes of X-ray emission are oriented perpendicular to the Galactic plane and centered on Sgr A\*. It is likely that these represent an outflow from the central parsec (Baganoff et al. 2003; Morris et al. 2003). Enhanced X-ray emission is also evident in the Northeast portion of the image, between the Galactic center and the Radio Arches region located  $\approx 3$  arcmin to the

north of the image (LaRosa et al. 2000a; Wang et al. 2002). This emission exhibits prominent He-like lines from Si and S, and low-ionization K- $\alpha$  emission from Fe (Park et al. 2004). Finally, a broad ridge of emission with low surface brightness is evident to the southwest (lower-right).

The hard band (4–8 keV) is also dominated by the Sgr A complex at the center of the image. At larger radii from the center, the most prominent features are filaments dominated by low-ionization Fe emission at 6.4 keV in the Northeast (Park et al. 2004), and a hard, continuum-dominated feature in the south (Sakano et al. 2003; Lu et al. 2003; Yusef-Zadeh 2003). These features have been removed from the image, as they were not included when we modeled the diffuse emission. Enhancements in the hard diffuse emission are also observed at the bipolar lobes, and in the Northeast.

In Figure 4, we display a smoothed, three color image of the field. The red band was made using photons between 0.5–2.0 keV, the green with 2.0–4.0 keV, and the

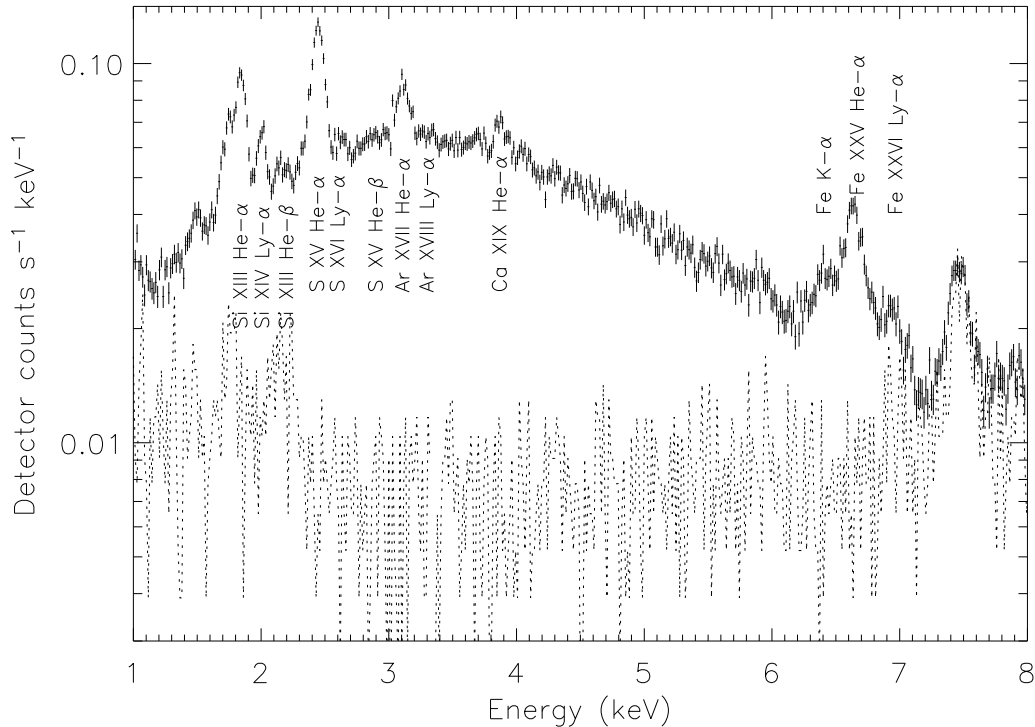


FIG. 5.— Spectrum of the diffuse emission from the Southeast dark region, before background subtraction. The instrumental background is indicated with the grey dashed line. Prominent lines from the diffuse emission are indicated.

blue with 0.4–8.0 keV. After removing the point sources, the image was adaptively smoothed using the algorithm described by Townsley et al. (2003). The red band contributes very little flux to the image, because the Galactic absorption column prevents us from receiving photons with energies  $\lesssim 2$  keV from the Galactic center. However, soft photons are received from the Sgr A complex, and from a bright, slightly extended feature of uncertain nature about  $6'$  north-northeast of Sgr A\*. All of the other features evident in the un-smoothed images are apparent in the smoothed image.

## 2.2. Spectra of the Diffuse Emission

We used the images in Figures 1–4 to select regions from which we extracted spectra of the diffuse emission. The regions are displayed with polygons in Figures 2 and 3. Five of the regions were chosen because they were particularly dark. The sixth was chosen from the bright region in the Northeast to help understand the nature of the surface brightness variations in Figure 4. We avoided the bipolar lobes and the ridge to the southwest, as they will be studied elsewhere.

In order to model the spectrum, for each region and each observation we computed an effective area function using the CIAO tool `mkwarf`, which accounts for the vignetting and satellite dither using the distribution of counts received in the extraction region. We then computed a weighted average of the effective area for each region, using as the weighting the number of counts in that region in each observation. Similarly, we computed a mean re-

sponse by averaging the response functions provided by Townsley et al. (2002b) from the range of detector rows covered by each region, also weighted by the number of counts in each observation. We estimated the background produced by particles impacting the detector using a 50 ks observation taken with the ACIS-I stowed out of the focal plane of the mirror assembly.<sup>6</sup> In order to account for spatial variations in the background across the ACIS-I chips, we extracted the background events from regions identical to those we used for the spectra of the diffuse emission. The background observations had the same CTI correction and filtering applied as we used for the source events. The area, average offset from the nominal aim point (Sgr A\*), total counts, and estimated instrumental background for each region are listed in Table 2. The instrumental background represents 20–25% of the total counts in the dark regions, but only 10% of the total counts in the bright region to the northwest. We note that the unresolved cosmic X-ray background contributes insignificantly to the diffuse emission. If we account for  $10^{23}$  cm<sup>-2</sup> of absorption through the Galaxy, and the fact that sources brighter than  $6 \times 10^{-15}$  erg cm<sup>-2</sup> s<sup>-1</sup> (2–8 keV; de-absorbed to match the deep-field surveys) should have been detected, less than 1% of the observed diffuse emission is from extragalactic background (e.g., Rosati et al. 2002).

Figure 5 displays the source and background spectrum of the Southeast region, which has the highest signal-to-noise of the dark regions. Many lines are detected in the spectrum: the He-like  $n = 2 - 1$  transitions of Si, S, Ar, Ca, and Fe; the He-like  $n = 3 - 1$  transitions of Si and S;

<sup>6</sup> <http://cxc.harvard.edu/contrib/maxim/stowed/>

the H-like  $n = 2 - 1$  transitions of Si, S, Ar, and Fe; low-ionization (“neutral”) Fe K- $\alpha$  at 6.4 keV; and an instrumental Ni line at 7.5 keV. Background-subtracted spectra are displayed in Figure 6; the absence of the instrumental Ni line at 7.5 keV indicates that the background subtraction was successful, whereas the other lines are clearly intrinsic to the diffuse emission.

Motivated by past investigations, we modeled the spectrum of the diffuse emission in two ways. First, we modeled the spectrum between 1–8 keV using two thermal plasma components. Second, we analyzed the spectrum between 4.5–8.0 keV in order to examine the properties of the iron lines.

### 2.2.1. Two- $kT$ plasma model

As pointed out by several authors (e.g. Koyama et al. 1986a; Yamauchi et al. 1996; Tanaka et al. 2000), the prominent line emission in the spectrum suggests that it originates from optically thin plasma, whereas the simultaneous presence of Fe with Si, S, and Ar suggests that the plasma has multiple temperature components. The plasma model we used (`apex`<sup>7</sup> in `XSPEC`; see also, e.g., Raymond & Smith 1977; Mewe, Lemen, & van den Oord 1986; Borkowski, Sarazin, & Blondin 1994) assumes that it is in collisional ionization equilibrium, and is able to self-consistently account for both the continuum emission and the lines from H-like and He-like species. The neutral Fe emission must be included ad-hoc as an additional Gaussian component.

Several assumptions were required for the model to reproduce the data. First, we only applied the model between 1.0 and 8.0 keV. Below this energy range the photon counts are dominated by foreground emission, while above this range the spectra are background-dominated. Second, we examined data taken in 2002 May from the on-board calibration sources (which produce lines at the K- $\alpha$  and K- $\beta$  transitions from Al, Ti, and Mn when the detector is exposed to them), and found that even after applying the CTI correction the observed line centroids were slightly below their expected values. The shift ranged from  $\lesssim 0.2\%$  near the detector read-out (at the top and bottom of Figure 1), up to  $\approx 0.9\%$  at the top of each CCD (the center of the image). Therefore, we allowed for a  $\approx 0.5\%$  shift in the energy scale in each spectrum. When fitting a Gaussian to the 6.4 keV line of Fe, the line centroids were allowed to vary once, and then were frozen. When using plasma models, the red-shift parameter was used to change the energy scale. Third, a 3% systematic uncertainty was added in quadrature to the statistical uncertainty on the count rate in order to account for uncertainties in the ACIS effective area. Finally, we found that we needed to allow the abundances of Si, S, Ar, Ca, and Fe to vary independently to obtain an adequate fit.

To account for absorption we assumed (1) that the entire region was affected by one column of material that represents the average Galactic absorption (modeled with `phabs` in `XSPEC`) and (2) that a fraction of each region was affected by a second column that represents absorbing material with a smaller filling factor along the line of sight (modeled with `pcfabs`). The absorption model roughly accounts for the fact that both the plasma and absorbing

material are distributed along the line of sight (see, e.g., Vollmer, Zylka, & Duschl 2003). The mathematical form of the model was

$$e^{-\sigma(E)N_{\text{H}}}([1 - f] + fe^{-\sigma(E)N_{\text{pc,H}}}), \quad (1)$$

where  $\sigma(E)$  is the energy-dependent absorption cross-section,  $N_{\text{H}}$  is the absorption column,  $N_{\text{pc,H}}$  is the partial-covering column, and  $f$  is the partial-covering fraction. The absorption was modeled using a separate factor (i.e., Equation 1) for each plasma component, although, aside from the quality of the fits, the basic results do not change if we use a single absorption factor for both plasma components. We note that for the soft plasma component the best-fit value of  $f$  approached 1 and was poorly constrained, so we fixed its value to  $f = 0.95$ .

Despite the complexity of the diffuse emission in the image, the spectra from all of the regions are basically described with the same collisional-equilibrium plasma model. We list the best-fit parameters for this model in each of the regions in Table 3, and display them in Figure 6. The uncertainties are  $1\sigma$ , derived from a search in chi-squared space with  $\Delta\chi^2 = 1.0$ . The value of  $\chi^2$  from some regions is formally poor, but this is not surprising given that the properties of the diffuse emission probably vary somewhat within each of the regions in Figures 2 and 3. We note that two-temperature non-equilibrium plasma models (`nei` and `vnei` in `XSPEC`; Masai 1984) did not reproduce the data nearly as well, as they yielded  $\chi^2_{\nu} > 1.5$  for all combinations of free parameters and absorption components. Moreover, the best-fit ionization parameters under those models were larger than  $10^{12} \text{ s cm}^{-3}$ , which reinforces the suggestion that the diffuse emission originates from plasma in thermal equilibrium.

The absorption columns derived are consistent with the expected Galactic values. The soft,  $kT \approx 0.8$  keV component has a total column of approximately  $5 \times 10^{22} \text{ cm}^{-2}$ , assuming that the partial-covering absorber affects 95% of the field. This indicates that only a small fraction of the soft diffuse emission originates in the foreground. The hot,  $kT \approx 8$  keV component is absorbed by about  $4 \times 10^{22} \text{ cm}^{-2}$  over the entire region, with additional absorption of  $\sim 5 \times 10^{23} \text{ cm}^{-2}$  affecting on order half of each region. The additional partial-covering absorption column is comparable to that which could be provided by the typical molecular clouds in the region,  $\sim 3 \times 10^{23} \text{ cm}^{-2}$  (Zylka, Mezger, & Wink 1990). The higher absorption toward the hard component is probably a selection effect, caused by the fact that no trace of the soft component could emerge from behind  $5 \times 10^{23} \text{ cm}^{-2}$  of absorption. The differences in the absorption column from field-to-field are not surprising given the non-uniform distribution of molecular clouds near the Galactic center.

The temperatures of the two plasma components,  $kT_{\text{cool}} = 0.7 - 0.9$  keV and  $kT_{\text{hot}} = 6 - 9$  keV, both differ from region to region. The temperature of the cooler component is well-constrained by the lines of Si, S, and Ar, and changes by at most 0.1 keV if a different absorption model is assumed. For example, assuming identical absorption for the cool and hot components, the derived temperature decreases to 0.6 keV for some of the regions, but the differences persist. Therefore, the dispersion in

<sup>7</sup> <http://cxc.harvard.edu/atombd>

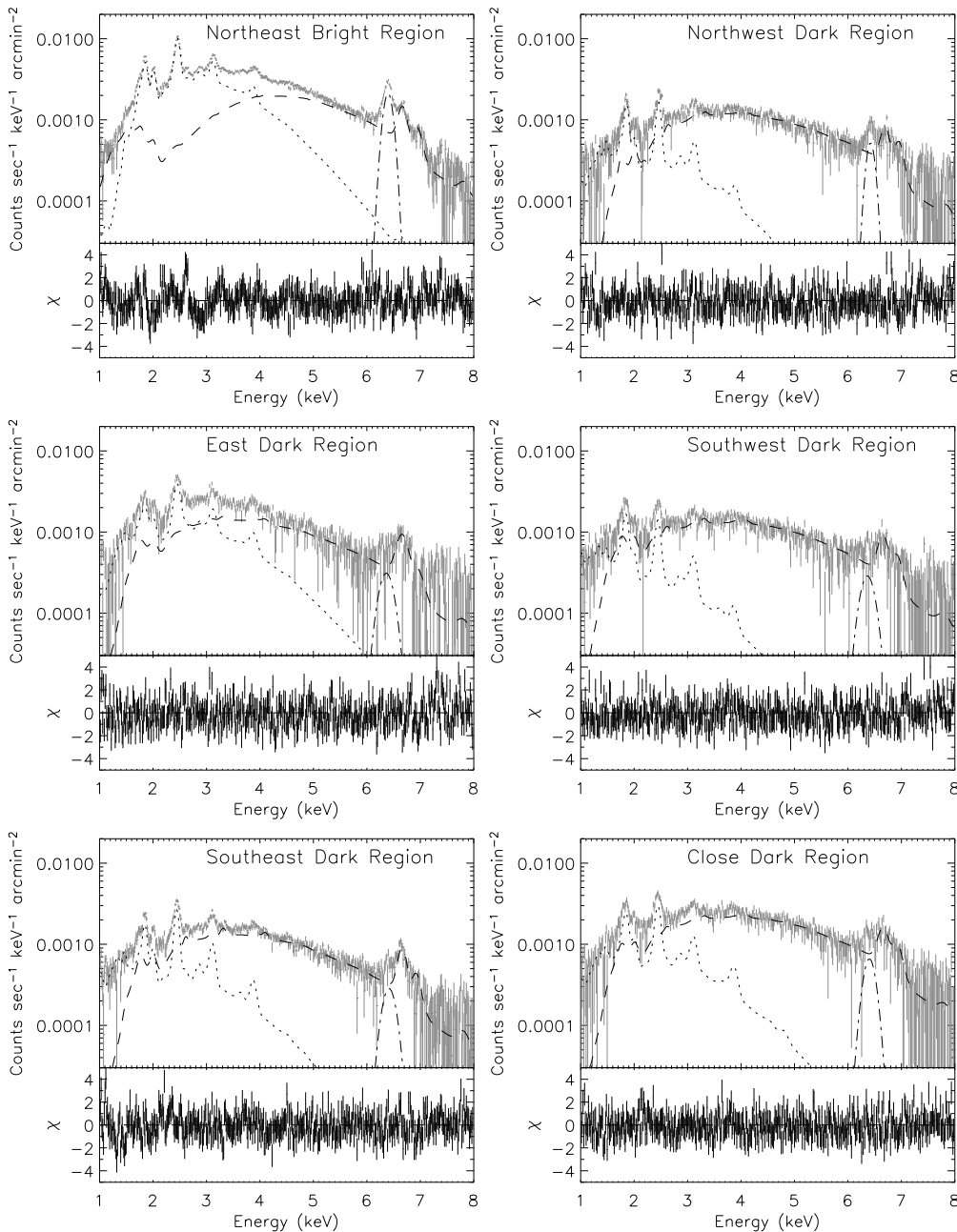


FIG. 6.— Background-subtracted spectra and best-fit two- $kT$  plasma model for each of the regions in Figure 2. The *dotted line* denotes the soft  $kT \approx 0.8$  keV plasma component, the *dashed line* indicates the hard  $kT \approx 8$  keV plasma component, and the *dot-dashed line* indicates the low-ionization Fe line emission.

the values of  $kT_{\text{cool}}$  are significant. On the other hand, the temperature of the hot component is determined both by the ratio of the H-like and He-like lines and by the continuum above 5 keV, and is more uncertain because the effective area of the detector there is smaller. Moreover,  $kT_{\text{hot}}$  differs by up to 2 keV when the absorption model is changed. For instance, when a single absorption factor of the form of Equation 1 is assumed,  $kT_{\text{hot}}$  increases to 10 keV because the continuum is inferred to be flatter. As

a result of the poorer constraint, the differences in  $kT_{\text{hot}}$  are only significant at the  $2\sigma$  level.

The fluxes of both spectral components also vary spatially. The emission measures are better correlated with the observed flux than are the temperatures, which suggests that the density or volume of the plasma is the most important factor determining the surface brightness of the diffuse emission. The flux from both plasma components is highest in the East and Northeast, as expected from the

images in Figures 2 and 3. The differences in the soft emission is the most dramatic: it is lowest in the Northwest, Southeast, and Southwest, 50% higher in the region close to the Galactic center, a factor of 3 higher in the East, and a factor of 9 brighter in the Northeast. On the other hand, the observed flux from the hard component differs by less than 10% in the four dark regions located at  $\sim 8'$  from Sgr A\*, and is only a 60% higher in the Close region and in the Northeast. The inferred de-absorbed hard fluxes differ even less, as the brightest regions produce only 25% more flux than the darkest.

Under the two-temperature plasma model, there appear to be significant ranges in the elemental abundances both when comparing individual elements, and when comparing the dark and bright regions. Unfortunately, we have found that the abundances of all of the metals can be made consistent with solar values if we add a third thermal plasma component with  $kT \approx 4$  keV to the model. Therefore, we must view the measured abundances with skepticism. It will be necessary to obtain spectra of the diffuse emission with higher energy resolution to draw firm conclusions about the metal abundances in the emitting material.

Finally, we note that the neutral Fe emission at 6.4 keV is a factor of 4 more intense in the Northeast than in the rest of the regions examined. This can be seen clearly in the equivalent width maps of Park et al. (2004). The strength of the 6.4 keV Fe emission clearly increases with that of the soft component of the diffuse emission in Figure 2, although it tends to appear in more strongly localized regions than the soft plasma. In fact, neutral Fe emission is responsible for the bright filamentary features in the Northeast of the hard image (Park et al. 2004).

These models are the simplest that we have found that reproduce the data. However, the intrinsic spectrum conceivably could be more complicated. For instance, if the low-ionization Fe line is produced as part of a reflection nebula, it should be accompanied by a scattered continuum component (e.g., Murakami et al. 2000). It has also been proposed that there is a non-thermal component to the spectrum between 2–8 keV, which represents a low-energy extension of the power-law emission seen above 10 keV (e.g., Valinia et al. 2000, but see Lebrun et al. 2004). Adding a power-law component with photon index  $\Gamma = 1.8 - 2.5$  does not significantly improve the fit, although the lower bound on the temperature of the hot plasma decreases to  $\approx 6$  keV. Likewise, adding a third plasma component does not improve the fit. None of the additional components change the basic conclusions that we present in Section 3.

### 2.2.2. Iron Emission

As we will discuss in Section 3, a thermal plasma containing He-like and H-like ions of Fe will inevitably be too hot to be bound to the Galactic plane, and will therefore require a very large amount of energy to sustain. This has led several authors to propose that much of the continuum and iron emission are produced by non-thermal processes. If this is the case, then the centroid energies, widths, and line ratios of the iron emission provide the best constraints on these models. Therefore, we have modeled the Fe K- $\alpha$ , He- $\alpha$ , and H- $\alpha$  line complexes with three Gaussians. The Fe He- $\alpha$  line is a combination of forbidden (6.63 keV),

inter-combination (6.67 keV), and resonance (6.70 keV) transitions that can not be resolved as separate lines with the ACIS-I. Likewise, the Fe H- $\alpha$  line (6.97 keV) should contain a contribution from the K- $\beta$  transition (7.03 keV), which has an intensity that is  $\lesssim 15\%$  of that of the K- $\alpha$  transition (e.g., Park et al. 2004). We modeled the continuum emission between 4.5–8.0 keV with a power law to facilitate the computation of equivalent widths. The resulting model parameters are listed in Table 4. The uncertainties are  $1\sigma$ , derived from a search in chi-squared space with  $\Delta\chi^2 = 1.0$  for the centroids, widths, and intensities, and  $\Delta\chi^2 = 2.3$  for the ratios of the intensities.

One of the best diagnostics of the non-thermal models are the centroid energies of the lines (e.g., Valinia et al. 2000; Masai et al. 2002). Due to the shift in the gain of the ACIS-I mentioned above, the observed energies of the Fe He- $\alpha$  and H- $\alpha$  lines are shifted to lower energies by  $\approx 0.5\%$ . These shifts are significant at the  $\lesssim 2\sigma$  level. However, the Fe K- $\alpha$  lines lie, within their uncertainties, right at the expected energy of 6.40 keV. If we account for a 0.5% shift to lower energies, its true centroid could be as high as 6.43 keV.

In some cases, non-thermal models for the iron emission also predict that the lines should be broadened (e.g., Tanaka et al. 1999). The widths of the K- $\alpha$  and He- $\alpha$  lines can only be constrained meaningfully with the two spectra that have the highest signal-to-noise, those from the Northeast and Southeast. In the Northeast, the Fe K- $\alpha$  line has a width of  $39 \pm 7$  eV, while in the Southeast its width is  $< 70$  eV. If the width in the Northeast is real, it would imply a velocity dispersion of  $\approx 2000$  km s $^{-1}$ . The Fe He- $\alpha$  line also appears to be resolved in the Northeast, with a width of  $50 \pm 20$  eV, while in the Southeast the upper limit to the width is 40 eV. In both cases, however, the width is consistent with the 70 eV separation between the recombination and forbidden lines. These widths are lower than those reported from ASCA data by Koyama et al. (1996) ( $75 \pm 10$  eV). The constraints from the remaining spectra are poorer, so we fixed the widths to 40 eV.

In all cases except the Northeast, the strongest of the iron lines is the He- $\alpha$  transition. It is a factor of 1.4–3.3 stronger than the K- $\alpha$  line, and a factor of 2.1–4.4 stronger than the H- $\alpha$  line. However, the uncertainties on the line ratios are large enough that we can not identify significant variations between the dark regions. The Northeast region stands out with a very strong K- $\alpha$  line with equivalent width of 570 eV. For comparison, the Fe K- $\alpha$  features studied by Park et al. (2004) had equivalent widths of 1 keV.

Overall, the properties of the iron emission are remarkably constant in the dark regions, with the only significant variations found in the bright regions to the Northeast, and to a lesser degree in the East.

### 2.3. Comparison to Point Sources

In this section, we examine three aspects of the point sources. First, we determine the amount of flux from detected point sources in each region, to evaluate whether the spatially varying detection threshold affects the amount of flux attributed to diffuse emission. Next, we compare the average spectrum of the detected point sources to that of the diffuse emission. Finally, we assume that unde-

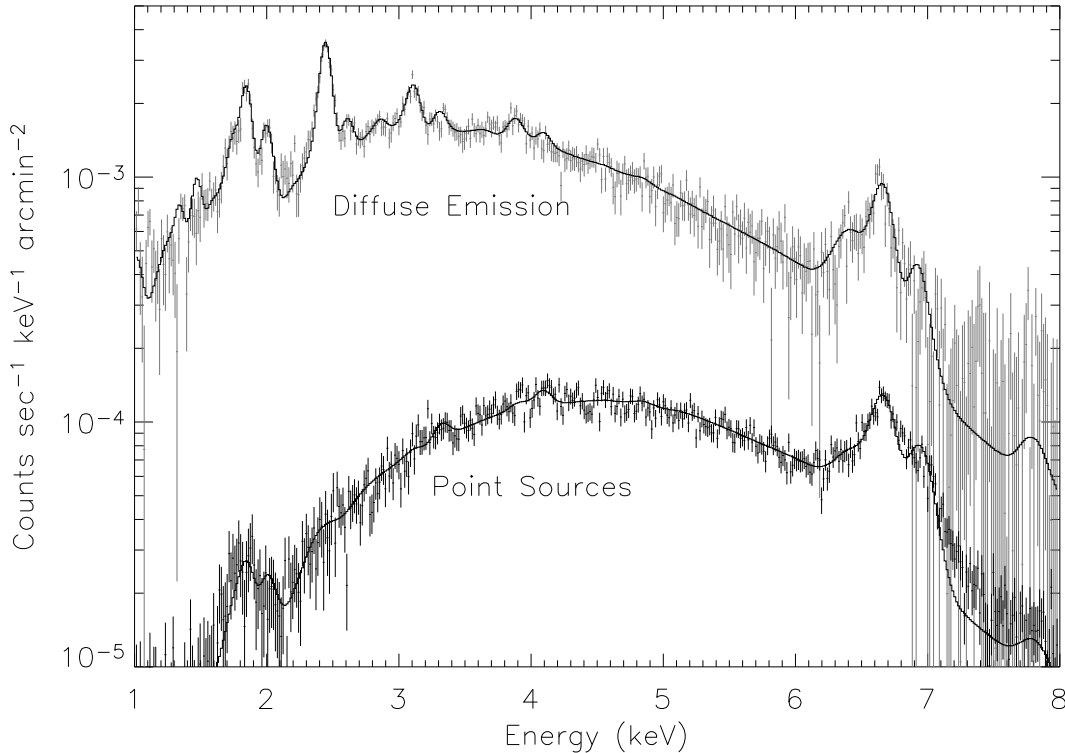


FIG. 7.— Background-subtracted spectrum of the diffuse emission from the southeast, compared to the average spectrum of the detected point sources in the entire  $17'$  by  $17'$  field. The spectrum of the diffuse emission has been normalized to the area from which it was extracted, while the spectrum of the point sources has been normalized to an area of  $17^2$  arcmin $^2$ . The detected point sources contribute no more than 20% of the total flux from the diffuse emission, even in the darkest regions of the image.

tected point sources have spectra identical to the detected sources, and determine the maximum flux that they could contribute to the diffuse emission.

In Muno et al. (2004), we examine the spectra of the point sources in considerable detail; the methods for extracting and combining the spectra of the point sources are described there. In brief, we extracted spectra from within the 90% contour of the PSF around each point source using the `acis_extract` routine from the Tools for X-ray Analysis (TARA).<sup>8</sup> We then summed the resulting spectra for each region. We computed the effective area functions for each source using `mkarf`, corrected them for the fraction of the PSF enclosed by each region and for the hydrocarbon build-up on the detectors. We then averaged the effective area weighted by the count rate from each source. Finally, we averaged the response functions that accompany the Townsley et al. (2002b) CTI-corrector from the location of each point source, again weighted by the counts from each source. In order to confirm that the point-source spectra were not contaminated by diffuse emission, we re-extracted the spectra for several hundred point sources from regions that enclosed only 50% of the PSF, and found that the resulting average spectrum was indistinguishable from that extracted from the 90% contour of the PSF.

Vignetting limits our ability to resolve point sources at large offset angles from the aim-point, so we first established that a failure to resolve point sources does not affect our estimates of the diffuse flux. To do so, we extracted

a summed spectrum from the point sources in each region. We used the diffuse emission from each region to estimate the background, and modeled the point source spectra with the same two- $kT$  model as for the diffuse emission. We list the surface brightness from detected point sources per square arcminute in Table 5, along with the total, soft, and hard flux from the diffuse emission. The flux from detected point sources is nearly identical in all of the dark regions located  $\approx 7.5'$  from the aim-point. Therefore, we have probably been equally successful at resolving point sources in each dark region. A larger flux from point sources is observed in the Northeast. Although this excess flux from point sources could indicate that there are more stellar X-ray sources in this region, it is more likely that we mistakenly identified small knots in the diffuse emission as point sources. Larger knots that could be identified as extended by eye were removed from the point source list. The flux from detected point sources close to the Galactic center is higher because (1) the angular resolution is better within  $5'$  of the aim point (Sgr A\*), so that it is possible to detect fainter sources, and (2) the surface density of point sources increases as  $\theta^{-1}$  toward Sgr A\*.

Next, we compared the spectrum of the point sources from the entire field to that of the diffuse emission. We found in Muno et al. (2004) that the averaged spectrum of the point sources changed only slightly when considering sources with intensities that ranged over a factor of

<sup>8</sup> <http://www.astro.psu.edu/xray/docs/TARA/>

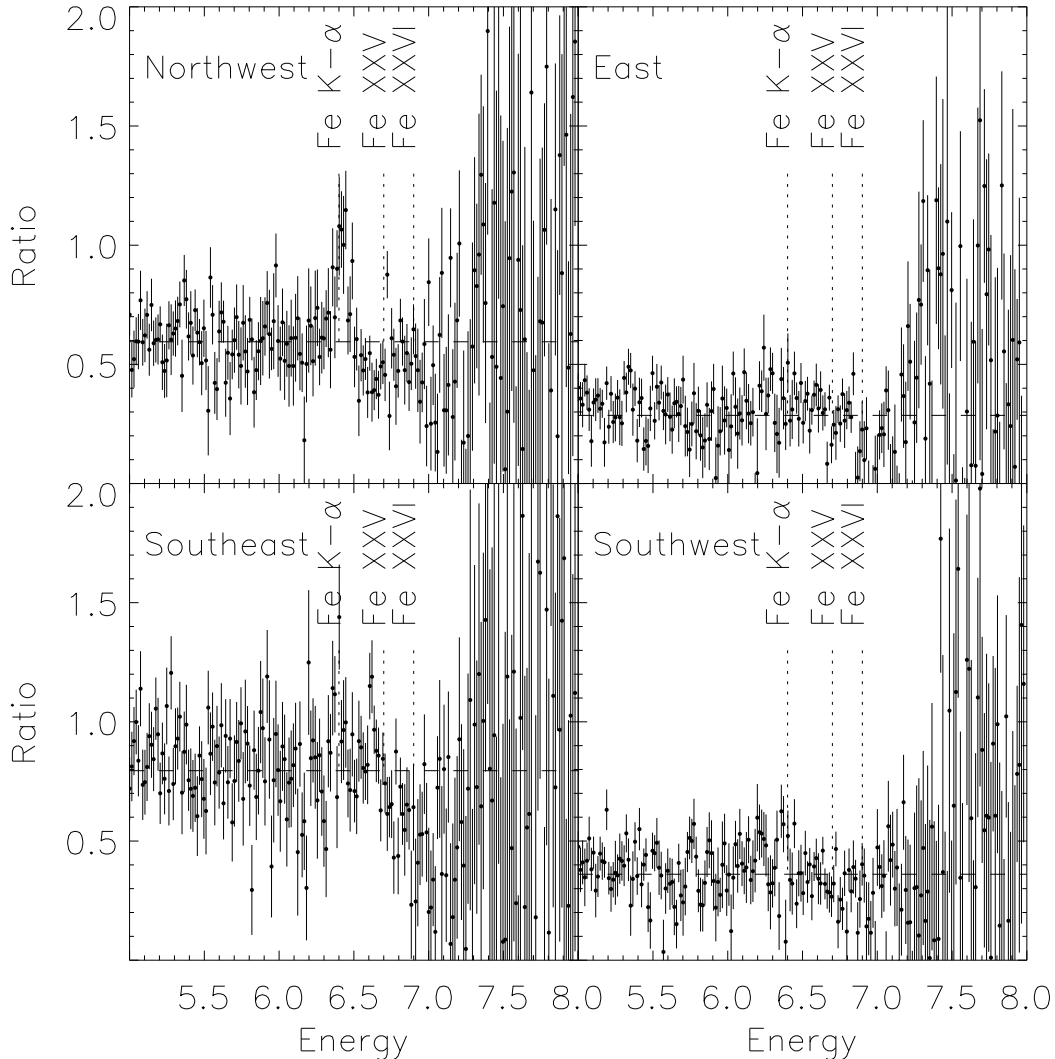


FIG. 8.— Ratios of the background-subtracted count spectra from diffuse emission to that from faint point sources. Ratios are displayed for the four dark regions located  $7'$  from Sgr A\*. The dashed line indicates the mean ratio between 5 and 7 keV. The ratio is nearly constant, which indicates that the spectral shapes are very similar. We note that the close region yields similar results, while the ratio from the Northeast exhibits significant deviations due to strong low-ionization iron emission.

$\sim 20$ , so we chose to compare the spectrum of point sources with fewer than 80 net counts to that of the diffuse emission. We used the spectrum of the diffuse emission from the entire field to estimate the background for the point sources. The average spectrum of the point sources and spectrum of the diffuse emission from the southeast are displayed in Figure 7, while the ratios between count spectra from the dark regions of diffuse emission to that from the point sources is displayed in Figure 8. As noted by Wang et al. (2002), the shapes and relative intensities of the He-like and H-like iron lines appear qualitatively similar in the point sources and diffuse emission. Under the two- $kT$  plasma model for the point sources, we find that the soft 0.8 keV component is heavily absorbed, so that it contributes only 3% of the total observed 2–8 keV flux. The hot 8 keV plasma component produces the remainder of the observed flux. Therefore, the near-absence of a soft component is the main reason that the point source spectra appear much harder.

In order to determine an upper limit to the amount of flux that undetected point sources can contribute to the diffuse emission, we have added a spectral component representing the point sources with fewer than 80 net counts to our two- $kT$  models for the diffuse emission. Only a constant normalization for the fiducial point source spectrum was allowed to vary, while the parameters of the spectral components representing the diffuse emission were allowed to vary as in Section 2.2.1. We increased the value of the constant normalization until  $\chi^2$  exceeded a threshold that corresponded to a 10% chance that the model and data were consistent. If the initial model was acceptable, the threshold was  $\chi^2 = 506$  for 456 degrees of freedom. However, in a couple of cases the initial model including the point source spectrum was unacceptable at the 90% confidence level (see Table 3), so we varied the normalization until  $\chi^2$  increased by  $\delta\chi^2 = (506 - 456) \cdot \chi^2/456$  (this is equivalent to inflating the assumed uncertainties to force  $\chi^2_{\nu}$  to equal 1 for the best-fit model).

The surface brightness of the diffuse emission that can be accounted for by undetected point sources is listed by region in Table 5. Undetected point sources may produce  $(0.7 - 1.5) \times 10^{-13}$  erg cm $^{-2}$  s $^{-1}$  arcmin $^{-2}$  in the regions 7' from the Galactic center, which is 35–80% of the total observed diffuse flux. The upper limits on the fluxes from undetected point sources are 2–5 times larger than the total flux from the observed point sources. We also list in Table 5 the flux from the soft and hard components that remains when an undetected point source contribution is subtracted. The reduction in inferred diffuse flux is most dramatic in the hard band: in the Southeast, Southwest, and Close dark regions, a hard diffuse component is not necessary if one includes a contribution of undetected point sources in the spectrum. Moreover, the remaining three regions in which undetected point sources cannot replace the hard component of the diffuse emission are also those regions in which the initial model for the diffuse emission (without the point source component) was formally unacceptable.

The similarity between the spectra of the point sources and diffuse emission suggests that all of the hard diffuse emission could be produced by point sources. However, in this case the larger hard flux in the Northeast would require that there are  $\approx 40\%$  more stellar X-ray sources per solid angle than in the dark regions at a similar offset from the Galactic center. We address this issue further in Section 3.4, where we estimate the number of undetected sources that would be required to produce the observed  $kT \approx 8$  keV diffuse emission.

### 3. DISCUSSION

As mentioned in the introduction, these *Chandra* observations of the diffuse emission within the 17' by 17' field around Sgr A\* provide three advantages over previous observations with *ASCA* (Koyama et al. 1996) and *BeppoSAX* (Sidoli & Mereghetti 1999): (1) the instrument does not produce line emission between 2–7 keV that could contaminate the spectrum and thereby produce ambiguities in the measured ionization state of the emitting medium (compare Figure 5 and, e.g., Tanaka 2002), (2) the long integration time allows us to measure the spectrum of the diffuse emission with high signal-to-noise on arcminute spatial scales (Figure 6), and (3) the high angular resolution of *Chandra* allows us to distinguish the truly diffuse emission from point sources, supernova remnants, and an apparent outflow from Sgr A\* (Figure 1).

The spectrum of the diffuse emission from the Galactic center is dominated by line emission from He-like and H-like Si, S, Ar, Ca, and Fe (Figure 5; see also Yamasaki et al. 1997; Tanaka 2002). These lines indicate that the diffuse emission results from a two-component collisionally-ionized plasma, with temperatures of  $kT_{\text{cool}} \approx 0.8$  keV and  $kT_{\text{hot}} \approx 8$  keV. The line energies and ratios are consistent with those expected from plasma in thermal equilibrium (compare Kaneda et al. 1997; Tanaka 2002). Therefore, in Section 3.1, we adopt the assumption of thermal equilibrium to examine the physical properties of the putative plasma responsible for the diffuse emission.

The main parameters of our spectral models, the temperature and emission measure of the putative plasma components, vary on scales of  $\approx 10$  pc. The properties of

the cool,  $kT_{\text{cool}} \approx 0.8$  keV component were determined primarily by the ratio of fluxes in the He-like and H-like transitions of Si and S (Figure 6), and were well-constrained. The temperature of the soft component of the plasma ranges between 0.7 to 0.9 keV, and its emission measure ranges between 1–24 cm $^{-6}$  pc (Table 3). The properties of the hot,  $kT_{\text{hot}} \approx 8$  keV component were derived from the ratio of fluxes in the He-like and H-like transitions of Fe, and by the shape of the continuum. This hard component is less well-constrained, because the instrumental effective area is much smaller near the Fe transitions at 6–7 keV than it is near the Si and S transitions at 1.5–2.5 keV. The temperature of the hard component ranges between 6–9 keV, but is consistent with a mean value of 8 keV at the  $2\sigma$  level. The emission measure ranges between 1.5–3.0 cm $^{-6}$  pc (Table 3). These spatial variations in the diffuse emission provide new insight into the origin of the putative plasma components that produce the diffuse emission, as we discuss in Sections 3.2 and 3.3.

Finally, we were able to separate the diffuse emission from point sources as faint as  $3 \times 10^{-15}$  erg cm $^{-2}$  s $^{-1}$ . We have already noted that the flux from the point sources detected in our *Chandra* image accounts for less than 10% of the diffuse emission from the Galactic center (Muno et al. 2003a). However, in the current paper we find that the average spectrum of the faintest point sources detected near Sgr A\* is remarkably similar to that of the hard component of the diffuse emission (see also Wang et al. 2002). The similarity is particularly striking between 6.5–7.0 keV, where there is strong emission from He-like and H-like Fe (Figure 7). As a result, if point sources that have not been detected have the same spectra as the detected ones, they could contribute up to 80% of the total 2–8 keV flux, and up to 100% of the hard component of the flux (Table 5). We address the plausibility that undetected point sources produce a significant fraction of the apparently diffuse flux in Section 3.4.

#### 3.1. Plasma Properties

The two- $kT$  plasma model provides as free parameters the temperature ( $kT$ ) and emission measure ( $K_{\text{EM}}$ ) of the plasma components. By assuming a depth for the emitting region, we can use these parameters to derive energies, densities, and time scales that can be used to understand the origin of the putative plasma. We list the properties for the putative soft and hard plasma components in Table 6. We assume a distance of 8 kpc to the Galactic center throughout the rest of the paper (McNamara et al. 2000).

The luminosity of the diffuse emission provides a lower limit to the amount of energy required to sustain it. We have computed the luminosity from the de-absorbed 2–8 keV fluxes in Table 3 by applying a bolometric correction that we determined by integrating the total flux from the *vapex* model in *XSPEC*; this is equivalent to using the cooling function in, for example, Raymond, Cox, & Smith (1976). The bolometric correction for the soft component is  $\approx 20$ , and for the hard component is  $\approx 2$ . Most of the extra luminosity lies between 0.1–2 keV, and would be easily detectable with *Chandra* were it not for the absorption toward the Galactic center. These corrections are uncertain by about 50%, as they depend upon the assumed elemental abundances. With these caveats in mind, we find

that the luminosities of the soft component range between  $(6 - 12) \times 10^{33}$  erg s<sup>-1</sup> arcmin<sup>-2</sup> in the darkest regions, up to  $9 \times 10^{34}$  erg s<sup>-1</sup> arcmin<sup>-2</sup> in the Northeast bright region. The luminosity of the hard component spans a smaller range, from  $(5 - 9) \times 10^{33}$  erg s<sup>-1</sup> arcmin<sup>-2</sup>.

The variations in the luminosity of the plasma are correlated with those in the emission measure,  $K_{\text{EM}} = \int n_e n_H dV$ , and therefore either the depths of the emitting regions or the densities of the plasmas vary spatially over the image in Figure 4. The depths of the emitting regions are probably somewhere between 10 pc, which corresponds to the approximate diameter of the extraction regions we used, and 250 pc, which corresponds to the 1.8° major axis of the elliptical region of 6.7 keV Fe emission region observed with *Ginga* (Yamauchi et al. 1990). We will take the geometric mean of these extreme values, and assume that the depth is 50 pc. We report each quantity in Table 6 with a scale factor  $d_{50}$  to account for possible variations in the depth of up to a factor of 5. This term can also account for the possibility that the filling factor of the plasma is less than unity. Because we are only interested in order-of-magnitude estimates, we assume that the plasma is pure hydrogen. The density of the plasma is then related to the emission measure by  $n_e = 0.1 d_{50}^{-1/2} K_{\text{EM}}^{1/2}$  cm<sup>-3</sup>. The mean density of the soft plasma is 0.1 cm<sup>-3</sup> in the darkest regions, and 0.5 cm<sup>-3</sup> in the bright region to the Northeast. The density of the hard plasma is near 0.1 cm<sup>-3</sup> over most of the image, and increases by a factor of 2 in the Northeast and within 4' of Sgr A\*. For comparison, Koyama et al. (1996) derive densities of 0.3–0.4 cm<sup>-3</sup> from their analysis of a larger, 1 square degree field observed with *ASCA*. This is probably because the larger field is dominated by bright regions similar to the Northeast region in our image, such as the Radio Arches region in the survey of Wang et al. (2002).

From the density and volume of the plasma, we can compute its total mass. The masses of both the soft and hard components in the dark regions are about  $1 d_{50}^{1/2} M_{\odot}$  arcmin<sup>-2</sup>. The density of soft plasma in the bright region is higher, so its mass is  $3 d_{50}^{1/2} M_{\odot}$  arcmin<sup>-2</sup>. The total mass of the plasma in the 17' by 17' field is about  $500 d_{50}^{1/2} M_{\odot}$ . For comparison, in the 1 square degree *ASCA* field, Koyama et al. (1996) derive a plasma mass of 2000–4000  $M_{\odot}$ , which is only slightly lower than our mass if one takes into account the difference in field-of-view.

The energy density of the plasma is  $U = \frac{3}{2} n k T$ , and so is proportional to  $d_{50}^{-1/2}$ . In the dark regions, the soft component has an energy density of  $3 \times 10^{-10}$  erg cm<sup>-3</sup>, or 200 eV cm<sup>-3</sup>. The hard component has an energy density of  $1 \times 10^{-9}$  erg cm<sup>-3</sup>, or 1 keV cm<sup>-3</sup>. The total energy per arcmin<sup>2</sup> is found by multiplying  $U$  by the plasma volume, and so is proportional to  $d_{50}^{1/2}$ . In the dark regions, the soft component has  $E = 2 \times 10^{48}$  erg arcmin<sup>-2</sup>, while the hard component has  $E = 2 \times 10^{49}$  erg arcmin<sup>-2</sup>. These values are nearly identical to those derived from the *ASCA* observations of Koyama et al. (1996). In the bright regions, the soft component has three times as much energy as it does in the dark regions, while the hard component contains only 50% more energy. The total thermal energy of the plasma in the image is over  $10^{51.8}$  erg.

Dividing the total energy of the plasma by its luminos-

ity yields the cooling time scale,  $t_{\text{rad}}$ . In the dark regions, the soft component cools in  $6 \times 10^6 d_{50}^{3/2}$  y. The bright region should cool more rapidly, in  $3 \times 10^6 d_{50}^{3/2}$  y, because  $t_{\text{rad}} \propto n^{-1}$ . The hard component cools in  $1 \times 10^7 d_{50}^{3/2}$  y.

However, it has been previously noted that an 8 keV plasma is too hot to be bound to the Galactic plane (e.g., Yamauchi et al. 1990; Kaneda et al. 1997; Yamasaki et al. 1997), so it is important to consider the amount of energy that could be lost as the plasma expands. If we use the Galactic potential from Breitschwerdt, McKenzie, & Völk (1991), we find that the escape velocity from the Galactic center ( $R \approx 20$  pc) is approximately 900 km s<sup>-1</sup>. This can be compared to the sound speed of the plasma  $c_s = (\gamma k T / \mu m_p)^{1/2}$ . If we assume  $\gamma = 5/3$  (for a monotonic, adiabatic gas) and  $\mu = 0.5$  (electrons and protons), the sound speed for the 0.8 keV plasma is  $\approx 500$  km s<sup>-1</sup>, and for the 8 keV plasma is  $\approx 1500$  km s<sup>-1</sup>. Therefore, only the cooler plasma is gravitationally bound to the Galaxy. However, in the absence of other confining forces, even the soft plasma could expand significantly; the contribution of the  $\approx 3 \times 10^7 M_{\odot}$  within the central 10 pc of the Galaxy (Laundhardt, Zylka, & Mezger 2002) is negligible when considering whether the plasma can expand, as the corresponding escape velocity from the central parsecs is only 150 km s<sup>-1</sup>. Using the potential in Breitschwerdt et al. (1991), the 0.8 keV plasma could expand to a height of several hundred parsecs.

Upper limits to the energy required to sustain the plasma components can be obtained by assuming that they expand adiabatically and form a wind from the Galactic center. Although computing the energy loss rate rigorously would require a full solution of wind equations such as those in Chevalier & Clegg (1985), we can make a rough estimate of it by assuming  $\dot{W}_{\text{exp}} = P dV/dt \approx P V^{2/3} c_s$ . For the soft component of the plasma, the energy loss rate is  $\sim 3 \times 10^{36}$  erg s<sup>-1</sup> arcmin<sup>-2</sup>, 300 times higher than the X-ray luminosity of the plasma. For the hot component of the plasma, this energy loss rate is  $\sim 1 \times 10^{38}$  erg s<sup>-1</sup> arcmin<sup>-2</sup>, or 4 orders of magnitude higher than its X-ray luminosity. Over the entire image, the upper limit to the power required is  $\sim 10^{40}$  erg s<sup>-1</sup>. The corresponding cooling time if the plasma is expanding is  $\sim 2 \times 10^4$  years for the  $kT \approx 0.8$  keV plasma, and  $\sim 6 \times 10^3$  years for the  $kT \approx 8$  keV plasma. These are much shorter than the radiative cooling time scales.

Even if external forces are on average sufficient to confine the diffuse plasma, any over-density in the plasma should be smoothed out in a short time by the differential rotation at the Galactic center. At 10 pc and for an enclosed mass of  $3 \times 10^7 M_{\odot}$  the orbital time scale is  $t_{\text{orb}} \approx 6 \times 10^5$  years. Therefore, differential rotation would smooth out any variations in the plasma properties with a radial extent  $\Delta R$  on a time scale of  $t_{\text{tidal}} \approx (R/\Delta R) t_{\text{orb}}$ . For parsec-scale features,  $t_{\text{tidal}} \approx 6 \times 10^6$  years, which is comparable to the cooling time of the soft plasma, but significantly shorter than the cooling time of the hard plasma.

### 3.2. Soft Component

The pronounced variations in the surface brightness of the soft,  $kT \approx 0.8$  keV component of the diffuse emission (Figure 2) have important implications for the spatial dis-

tribution and age of the putative plasma that produces it. The fact that the spatial variations are much more pronounced in the soft emission than in the hard (Table 6) suggests that the soft plasma occupies a much smaller volume. Indeed, if we assume that the soft and hard plasma are in pressure equilibrium, then the filling factor of the soft plasma would have to be roughly 1–10% of that of the hard plasma. At the same time, any over-density in the soft plasma is unlikely to survive very long, because the differential rotation of the Galactic center should shear apart any coherent features. For example, the bright diffuse emission in the Northeast has an angular extent that corresponds to a size of  $\approx 20$  pc, and so differential rotation should dissipate it within the orbital time scale of  $6 \times 10^5$  y.

The youth and small filling factor of the  $kT \approx 0.8$  keV plasma are easily understandable if it is produced by supernova remnants. This is the common explanation for the origin of similar soft diffuse emission that is observed throughout the Galactic disk, because supernova remnants are often observed to have spectra consistent with  $\sim 1$  keV plasma (e.g., Kaneda et al. 1997). Supernova are also the largest known source of energy for heating the ISM (Schlickeiser 2002), and can easily provide enough energy to heat the diffuse soft plasma. If we assume that the dominant cooling mechanism for the soft plasma is radiative, then the energy input required to sustain it is only  $\approx 3 \times 10^{36}$  erg s $^{-1}$  for the inner 20 pc of the Galaxy. If, on analogy with the conclusions of Kaneda et al. (1997) for the Galactic disk, we assume that  $\sim 1\%$  of the  $10^{51}$  erg of kinetic energy per supernova heats the soft plasma in our image, then it could be sustained by supernova occurring at a rate of one every  $10^5$  y. This is not unreasonable, because the total Galactic supernova rate is thought to be on order 1 per 100 y, and the inner 20 pc of the Galaxy contains approximately 0.1% of the Galactic mass (Launhardt, et al. 2002), so the expected rate in this field is also about one supernova per  $10^5$  y. Moreover, Sgr A East (Maeda et al. 2002) and the radio wisp 'E' (Ho et al. 1985) are already thought to be remnants of recent supernova, so it seems likely that the inner 20 pc of the Galaxy has experienced a supernova rate at least this high.

It is also possible that the winds from young, massive Wolf-Rayet and early O stars could contribute to the  $kT \sim 0.8$  keV plasma. A typical WR star can lose mass at a rate of  $\dot{M} \approx 10^{-5} M_{\odot} \text{ y}^{-1}$  with a velocity of  $v \approx 2000$  km s $^{-1}$  (e.g. Leitherer, Robert, & Drissen 1992; Stevens & Hartwell 2003). The kinetic energy of such a wind is  $3 \times 10^{37}$  erg s $^{-1}$ . X-rays are produced by internal shocks in the winds of individual stars, but diffuse X-rays are only produced by the large shocks that occur when winds from clusters of these stars encounter the interstellar medium. In observations of massive star clusters, about 10% of the wind kinetic energy is converted into X-rays (Stevens & Hartwell 2003; Townsley et al. 2003). Therefore, a single WR and/or early O star could in principle produce the soft component of the diffuse emission. However, extended X-ray emission from massive stars is usually only associated with young stellar clusters that contain several massive stars within a core radius of  $\sim 2$  pc, which typically produce X-rays in a region only  $\sim 3$  pc in radius (Townsley et al. 2003). Therefore, the X-ray emission from the winds

of massive stars is likely to only be important within an arcminute of any as-yet-undiscovered star clusters.

The detection of strong  $kT \approx 0.8$  keV emission to the Northeast of the Galactic center is also consistent with our assumption that the soft plasma originates from supernovae and winds from massive stars. The Northeast region possesses several interesting properties that may be related to the enhanced diffuse X-ray emission: it contains large amounts of molecular gas (Dahmen et al. 1998, Tsuboi, Handa, & Ukita 1999; Mezger, Duschl, & Zylka 1996); it is located between young, massive star clusters at the Galactic center (Krabbe et al. 1995; Paumard et al. 2001) and the Radio arches region (Figer et al. 1999), and it is the site of the strongest low-ionization Fe emission (Park et al. 2004). The mere presence of molecular clouds is clearly not sufficient for forming the soft diffuse and 6.4 keV Fe emission, as molecular clouds are also evident in the Southeast, without any corresponding enhancement in the iron emission (Park et al. 2004). Given the arguments for the origin of the soft plasma above, it is more likely that both the soft diffuse emission and the neutral Fe emission are associated with recent star formation. For instance, a Type II supernova in the Northeast could produce both the bright, soft diffuse emission and the neutral Fe emission (e.g., Maeda et al. 2002; Bykov 2002). Outside of the Galactic center, the most similar region may well be the Carina Nebula, which exhibits  $\approx 2 \times 10^{35}$  erg s $^{-1}$  of X-rays from the outflow around  $\eta$  Car, the WR and O stars in the cluster Trumpler 14, and diffuse emission that may have resulted from recent supernovae (Seward & Chlebowski 1982).

### 3.3. Hard Component

The hard,  $kT \approx 8$  keV emission is distributed much more uniformly than the soft, but its intensity is still correlated with that of the soft emission. The correlation between the hard and soft emission suggests that they are produced by related physical processes. The relative uniformity of the hard emission may result from its higher sound speed, which would cause over-dense regions of  $kT \approx 8$  keV plasma to expand on a time scale of  $\sim 10^4$  y.

However, the  $kT \approx 8$  keV plasma is somewhat hotter than is usually observed from either supernova remnants or clusters of WR and early O stars (see, e.g., Maeda et al. 2002; Townsley et al. 2003). Moreover, the sound speed of the hot plasma is larger than the escape velocity from the Galactic center, and therefore the energy required to sustain the expanding  $kT \approx 8$  keV plasma within the image in Figure 4 is  $\sim 10^{40}$  erg s $^{-1}$ . This energy is four orders of magnitude larger than that required to sustain the  $kT \approx 0.8$  keV plasma (which probably does not cool by expanding), and is equivalent to the entire kinetic energy of one supernova occurring every 3000 y. This makes it difficult to understand the origin of this putative hot plasma, because supernovae are assumed to be the largest source of heat for the ISM. Moreover, using the values in Table 6, the plasma flowing out from within the inner  $R = 20$  pc of the Galaxy would carry away a mass of roughly  $\dot{M} \sim 4\pi R^2 m_p n c_s \sim 10^{-2} M_{\odot} \text{ y}^{-1}$ . This mass loss rate is also equivalent to that from one supernova occurring every 3000 y. Finally, this  $kT \approx 8$  keV diffuse

emission is observed from throughout the Galactic disk, so the mechanism producing it must be widespread. In particular, the hot diffuse emission is probably not produced by the super-massive black hole at the Galactic center, Sgr A\*.

Several mechanisms have been proposed to explain the origin of the  $kT \approx 8$  keV component of the Galactic diffuse emission. One possibility is that the hard plasma is heated by magnetic reconnection that is driven by the turbulence that supernovae generate in the ISM (Tanuma et al. 1999). Magnetic connection could heat the plasma to  $nkT \sim B^2/8\pi$ , or, for  $n \approx 0.1 \text{ cm}^{-3}$  and  $B \approx 0.2$  mG (Table 6),  $kT \sim 8$  keV. Fields of comparable strength are inferred to exist near the Galactic center (e.g., Serabyn & Morris 1996). Moreover, Tanuma et al. (1999) also pointed out that with the right geometry, the same fields would also be strong enough to confine the  $kT \approx 8$  keV plasma, thus possibly reducing the amount of energy required to sustain it. Unfortunately, the magnetic fields toward the Galactic center appear unlikely to confine the hot plasma. Individual magnetic flux tubes are observed as synchrotron-emitting radio filaments oriented perpendicular to the Galactic plane (Yusef-Zadeh & Morris 1987; LaRosa et al. 2000a). These filaments seem to be interacting with molecular clouds in the region, and are therefore thought to have pressures comparable to those of the turbulent molecular clouds, so that  $B \approx 1$  mG (compare Serabyn & Morris 1996; Dahmen et al. 1998). However, it is not clear whether the filaments represent only a small fraction of vertical fields that pervade the Galactic center (Serabyn & Morris 1996; Chandran, Cowley, & Morris 2000), or whether they represent purely local magnetic features (Chevalier 1992; LaRosa, Lazio, & Kassim 2001; Yusef-Zadeh 2003). There is also a toroidal component observed through polarization measurements that dominates within molecular clouds (Novak et al. 2003). However, the Zeeman-splitting measurements of Uchida & Güsten (1995) placed upper limits of  $\approx 0.3$  mG to the strength of any arcminute-scale ordered fields along the lines-of-sights towards most of the molecular clouds near the Galactic center; the only Zeeman measurements that reveal fields  $\gtrsim 1$  mG are toward the circum-nuclear disk (Killeen, Lo, & Crutcher 1992). Taken together, these observations suggest that the magnetic fields are predominantly vertical at the Galactic center, with a toroidal component produced by orbital shear in the molecular clouds (Uchida & Güsten 1995; Chandran et al. 2000; Novak et al. 2003). Therefore, any hot plasma at the Galactic center would be able to escape vertically away from the plane, thus forming a wind or fountain of plasma (e.g., Breitschwerdt et al. 1991).

Another class of hypotheses assume that the hard component of the Galactic diffuse emission is produced by non-thermal processes associated with supernova shocks. For instance, low-energy ( $< 1$  MeV) cosmic rays could interact with the neutral ISM to produce continuum emission through bremsstrahlung radiation and line emission through charge-exchange interactions (e.g., Valinia & Marshall 1998; Tanaka et al. 1999; Valinia et al. 2000). The cosmic-ray electrons could be accelerated by supernova or young pulsars (e.g., Schlickeiser 2002). Originally, this model was attractive because it could also explain the non-thermal X-ray emission observed above 10 keV. However,

observations with *INTEGRAL* have resolved  $\approx 85\%$  of the emission above 20 keV into discrete point sources (Lebrun et al. 2004). Moreover, neither non-thermal electrons nor protons are efficient at producing bremsstrahlung radiation, so the energy required to produce the observed diffuse emission is nearly as large as that required to replenish a continually-expanding thermal plasma (Dogiel et al. 2002). Finally, the model presented by Valinia et al. (2000) does not predict the presence of the Fe H- $\alpha$  line at 6.9 keV, which is clearly evident in our *Chandra* spectra (Figure 5 and Table 4).

Alternatively, the hard diffuse emission could originate from a quasi-thermal plasma that is generated by supernova shocks that propagate through the cooler 0.8 keV plasma (Dogiel et al. 2002; Masai et al. 2002). This process is a factor of  $\sim 30$  more efficient at generating X-rays than is an expanding thermal plasma. Therefore, an energy input of  $5 \times 10^{38} \text{ erg s}^{-1}$ , or the kinetic energy of one supernova occurring every  $7 \times 10^4$  y, is required to produce the observed hard diffuse emission. However, neither of the two model spectra presented by Masai et al. (2002) are entirely consistent with the data in Table 4. Their models predict that Fe K- $\alpha$  lines should be of comparable strength as the He- $\alpha$  line at 6.7 keV, whereas in all of the dark regions the Fe K- $\alpha$  lines are a factor of 2–3 weaker, and in the Northeast bright region it is a factor of 1.8 stronger. Their models also predict that the Fe He- $\alpha$  lines should be a factor of 1.7–2.5 stronger than the Fe H- $\alpha$  lines (depending upon whether the background plasma has a temperature of 0.6 or 0.3 keV), whereas we find values that are generally higher, albeit only at the 1– $2\sigma$  level in each case. Finally, they predict that if the shocks form in a cool (0.3 keV) background plasma, then the low-ionization Fe line should have a centroid near 6.5 keV. The observed centroids are consistent with 6.4 keV, and values as high as 6.5 keV are excluded at the  $\gtrsim 6\sigma$  level in the Southwest and Northeast. Therefore, the non-thermal models that have been published to date are challenged by the remarkable similarity between the observed spectrum and that expected from a  $kT \approx 8$  keV plasma in thermal equilibrium. However, further exploration of the parameter space of the non-thermal models is needed to confirm or refute them definitively.

### 3.4. The Number of Undetected Point Sources

The spectrum of the  $kT \approx 8$  keV plasma is also very similar to that of the faintest detected point sources. Therefore, in this section we use the  $\log(N) - \log(S)$  distribution from Equation 5 in Munro et al. (2003a) to compute the number of point sources that would be required to produce the hard diffuse emission in the darkest region of the image:  $1.7 \times 10^{-13} \text{ erg cm}^{-2} \text{ s}^{-1} \text{ arcmin}^{-2}$  in the Northwest. The  $\log(N) - \log(S)$  distribution allows us to compute the surface density of sources down to a limiting flux  $S$ . Adapting the results of Munro et al. (2003a), we find:

$$N(S) = \begin{cases} \frac{20}{\theta} \left( \frac{S}{3 \times 10^{-15}} \right)^{-1.7 \pm 0.2} & S < 6 \times 10^{-15} \\ \frac{5}{\theta} \left( \frac{S}{6 \times 10^{-15}} \right)^{-1.34 \pm 0.08} & S > 6 \times 10^{-15}. \end{cases} \quad (2)$$

We have made several modifications to this equation from the original version. First, we have included a factor  $\theta$  for the offset from Sgr A\* in arcminutes, which accounts for

the decrease in surface density of the point sources within  $9'$  from the Galactic center. Second, we have converted the photon fluxes in Muno et al. (2003a) to energy fluxes by assuming  $1 \text{ photons cm}^{-2} \text{ s}^{-1} = 8 \times 10^{-9} \text{ erg cm}^{-2} \text{ s}^{-1}$  (2.0–8 keV), which is appropriate for a  $\Gamma = 0.5$  power-law spectrum absorbed by a  $6 \times 10^{22} \text{ cm}^{-2}$  column of gas and dust. Finally, we have normalized the distribution in Equation 2 to the surface density at  $\theta = 1'$ , whereas Equation 5 from Muno et al. (2003a) was normalized to the density at  $4.5'$ . We can then obtain the total flux from point sources ( $F_{\text{ps}}$ ) in any given region by integrating the power laws in Equation 2:

$$N_o S_o \frac{\alpha}{\alpha - 1} \left[ \left( \frac{S_{\text{min}}}{S_o} \right)^{-(\alpha-1)} - \left( \frac{S_{\text{max}}}{S_o} \right)^{-(\alpha-1)} \right] \times \int \frac{1}{\theta} dA. \quad (3)$$

Here,  $\alpha$  is the power-law slope,  $S_o$  is the scale factor for the flux, and  $N_o$  is the normalization of the power law, all from Equation 2.  $S_{\text{min}}$  and  $S_{\text{max}}$  are the bounds on the point-source flux over which the total flux  $F_{\text{ps}}$  is computed. For the bright end of the distribution in Equation 2, we assume  $S_{\text{max}}$  is  $4 \times 10^{-13} \text{ erg cm}^{-2} \text{ s}^{-1}$ , which is the brightest point source that we observe in the image; the values of  $F_{\text{ps}}$  are not very sensitive to this assumed upper bound. The number of point sources in a region is then found by inserting the assumed value of  $F_{\text{ps}}$  and solving for  $S_{\text{min}}$  in Equation 3, and then inserting  $S_{\text{min}}$  into Equation 2. Based on the observed hard diffuse and point source flux in the Northwest (Table 2 and 5), we take  $F_{\text{ps}} = 4 \times 10^{-12} \text{ erg cm}^{-2} \text{ s}^{-1}$ , and find  $S_{\text{min}} = 1 \times 10^{-16} \text{ erg cm}^{-2} \text{ s}^{-1}$ . Using this limiting flux in the  $\log(N) - \log(S)$  distribution, we would predict a surface density of 800 undetected sources  $\text{arcmin}^{-2}$  at an offset of  $4.5'$  from Sgr A\*, or a total of  $2 \times 10^5$  sources within 20 pc ( $9'$ ) of Sgr A\*.

There is no known class object of that could account for that large a number of hard X-ray sources at the Galactic center. In fact, the total stellar mass within the inner 20 pc of the Galaxy is only  $\sim 10^8 M_{\odot}$  (Launhardt, et al. 2002), so in order to account for the diffuse emission,  $\sim 0.2\%$  of all stellar sources would have to be hard X-ray sources with  $L_X > 3 \times 10^{29} \text{ erg s}^{-1}$ . The only plausible candidates for such a large population of hard X-ray sources are cataclysmic variables (CVs) and young stellar objects (YSOs). We can estimate the number of CVs within 20 pc of the Galactic center by scaling their local density by the relative stellar mass density. Based upon the mass model of Launhardt, et al. (2002), the stellar density in the inner 20 pc is  $1000 M_{\odot} \text{ pc}^{-3}$ , compared to a local density of  $0.1 M_{\odot} \text{ pc}^{-3}$ . The local space density of CVs is at most  $3 \times 10^{-5} \text{ pc}^{-3}$  (Warner 1995; Schwöpe et al. 2002), so the space density at the Galactic center should be less than  $0.03 \text{ pc}^{-3}$ . Therefore, we expect only  $\sim 10^4$  CVs there, which is an order of magnitude smaller than the number of point sources needed to explain the hard component of the diffuse emission.

The number of YSOs would depend on the recent formation rate for low-mass stars. If stars have formed steadily over the  $\sim 10$  Gyr lifetime of the Galaxy, then the  $\sim 10^8 M_{\odot}$  of stars within the inner 20 pc would have formed at a rate of  $\sim 10^{-2} \text{ y}^{-1}$ , which would imply

that there should be  $\sim 10^4$  stars younger than 1 Myr old. This number is comparable to the limit obtained from the fact that only  $\sim 5$  hard X-ray sources in our field exhibit flares with luminosities and durations that are similar to one seen from YSOs (Muno et al., in preparation 2004). About 0.1% of YSOs exhibit flares that would have been detectable from the Galactic center, which suggests that  $\lesssim 5000$  YSOs lie near the Galactic center (Feigelson 2004; Grosso et al. 2004), which is still far too few to produce the hard diffuse emission.

Other X-ray sources that are similarly abundant are unlikely to contribute to the hard component of the diffuse emission because their luminosities are too low or their spectra are too soft. For instance, although RS CVns are at least as numerous as CVs (Favata, Micela, & Sciortino 1995), they have thermal spectra with  $kT < 2$  keV (Singh, Drake, & White 1996). Likewise, while isolated neutron stars accreting from the interstellar medium could make up  $\sim 1\%$  of the mass of the Galactic center (Zane, Turolla, & Treves 1996), they must be less luminous than  $10^{29} \text{ erg s}^{-1}$ , or else many thousands of similar systems would have been detected in the local Galaxy in the *ROSAT* All-Sky survey (Perna et al. 2003). In contrast, less than a dozen candidate isolated neutron stars were identified with *ROSAT*. Therefore, if the diffuse emission is produced by undetected point sources, they would have to belong to a population of sources that has not yet been identified.

#### 4. CONCLUSIONS

Using a 600 ks exposure with the ACIS-I aboard *Chandra*, we have studied the spectrum of diffuse X-ray emission from several regions within a projected distance of 20 pc of Sgr A\*. The spectrum of the diffuse emission exhibits He-like and H-like lines from Si, S, Ar, Ca, and Fe, as well as a prominent low-ionization Fe line. If the spectrum is modeled as originating from diffuse plasma, two components with temperatures of 0.8 keV and 8 keV are required, along with line emission from low-ionization Fe at 6.4 keV. The energies and flux ratios of the lines from both temperature components are consistent with emission from plasmas in collisional ionization equilibrium.

In Table 7, we provide a summary of the origins of the X-ray emission between 2–8 keV from the inner 20 pc of the Galaxy. By far the largest contribution to the luminosity of the Galactic center is from diffuse emission. In comparison, detected point sources contribute only 10% to the luminosity of the Galactic center, while discrete filamentary features contribute less than 5% of the total luminosity of the inner 20 pc of the Galaxy. These results are potentially useful for understanding the origin of diffuse X-ray emission from distant galaxies with quiescent central black holes. However, it is important to note that these observations of the Galactic center are strongly affected by interstellar absorption with a column density of at least  $6 \times 10^{22} \text{ cm}^{-2}$ . Therefore, the cool emission with  $kT \lesssim 0.5$  keV that produces most of the 0.5–8.0 keV flux from distant galaxies is obscured at the Galactic center. At the same time, *Chandra* observations of other galaxies are not sensitive to the  $kT \approx 8$  keV plasma that dominates the flux we observe from the Galactic center, because this hard emission has a much lower surface brightness than the  $kT \lesssim 1$  keV emission where the *Chandra* effective area is

largest (0.5–3 keV), and it is difficult to resolve from bright X-ray binaries. Thus, these observations of the Galactic center provide a unique view of the hottest components of the ISM of galaxies.

The properties of the soft,  $kT \approx 0.8$  keV plasma component of the diffuse emission vary significantly across the image, both in temperature between 0.7 and 0.9 keV, and in surface brightness between  $2 \times 10^{-14}$  and  $1.7 \times 10^{-13}$  erg  $\text{cm}^{-2} \text{s}^{-1} \text{arcmin}^{-2}$ . The variation in the properties of the soft plasma suggest that it is relatively young, because differential rotation at the Galactic center should destroy any coherent features within  $< 10^6$  y. Supernovae probably supply most of this energy, although the winds from WR and early O stars could also contribute. Within the inner 20 pc of the Galaxy, the  $\approx 3 \times 10^{36}$  erg  $\text{s}^{-1}$  lost by the plasma through radiative cooling could be replaced by 1% of the kinetic energy of one supernova occurring every  $\sim 10^5$  y. The inner 20 pc of our Galaxy contains about 0.1% of its total mass, so assuming that one supernova occurs every 100 y in the Galaxy, this rate is roughly consistent with that expected near the Galactic center.

The hard component of the diffuse emission is more spatially uniform than the soft, but the intensities of the two components are still correlated. Although this might suggest a common origin for the two plasma components, supernovae and massive stars are not usually observed to produce plasma with  $kT \gtrsim 3$  keV. This hard emission is distributed throughout the Galactic plane, so it is not likely to be associated with an outburst from Sgr A\*. Instead, the hard emission could result from a  $kT \approx 8$  keV plasma that is heated indirectly by massive stars and supernova remnants, which, for example, could drive reconnection in the magnetic fields near the Galactic center (Tanuma et al. 1999). However, a 8 keV thermal plasma would freely expand away from the Galactic center, and would require  $\approx 10^{40}$  erg  $\text{s}^{-1}$  to sustain. This is equivalent to the entire kinetic energy of one supernova every 3000 years, which is a much larger rate than usually assumed for supernova. Supernovae are the most energetic

source of heat for the ISM, so if the hard diffuse emission is produced by a  $kT \approx 8$  keV plasma, it would imply that there is a significant shortcoming in our understanding of heating mechanisms for the ISM.

Alternative explanations for the hard diffuse emission that were intended to lessen the energy required are equally unsatisfying. The suggestion that the hard diffuse emission originates from undetected stellar X-ray sources is unlikely because there is no known class of source that are numerous enough, bright enough, and hot enough to produce the observed flux of  $kT \approx 8$  keV diffuse emission. Likewise, if the hard diffuse emission originates from non-thermal processes, such as the shocks that accelerate cosmic rays, the energies and ratios of the intensities of the line emission should deviate measurably from the values expected for a plasma in thermal equilibrium (e.g., Masai et al. 2002). These deviations are not observed in our *Chandra* observations, which presents a challenge to the current non-thermal models.

Further observations should clarify the nature of the diffuse X-ray emission from the Galactic center. X-ray missions with higher spectral resolution, such as ASTRO-E 2, will be able to better-constrain the properties of the putative diffuse plasma by resolving the individual transitions of He-like and H-like Fe, and possibly measuring the velocity dispersions of the Fe ions themselves. Alternatively, a future hard X-ray survey, such as EXIST, could identify a heretofore unknown population of numerous, faint, hard X-ray sources that may be responsible for producing the  $kT \approx 8$  keV diffuse emission.

We are grateful to F. Paerls and T. Treu for helpful discussions as this paper was taking shape, and the referee for insightful comments that aided us in clarifying our conclusions. MPM was supported by a Hubble Fellowship from the Space Telescope Science Institute, which is operated by the Association of Universities for Research in Astronomy, Inc., under NASA contract NAS 5-26555.

## REFERENCES

- Baganoff, F. K. et al. 2003, *ApJ*, 591, 891  
 Bamba, A., Ueno, M., Koyama, K., & Yamauchi, S. 2003, *ApJ*, 589, 253  
 Breitschwerdt, D., McKenzie, J. F., & Völk, H. J. 1991, *A&A*, 245, 79  
 Borkowski, K. J., Sarazin, C. L., & Blondin J. M. 1994, *ApJ*, 429, 710  
 Bykov, A. M. 2002, *A&A*, 390, 327  
 Chandran, B. D. G., Cowley, S. C., & Morris, M. 2000, *ApJ*, 528, 723  
 Chevalier, R. A. 1992, *ApJ*, 397, L39  
 Chevalier, R. A. & Clegg, A. W. 1985, *Nature*, 317, 44  
 Dahmen, G., Hüttemeister, S., Wilson, T. L., & Mauersberger, R. 1998, *A&A*, 331, 959  
 Dogiel, V. A., Inoue, H., Masai, K., Schönfelder, V., & Strong, A. W., 2002, *ApJ*, 581, 1061  
 Draine, B. T. 2003, *ApJ*, 598, 1026  
 Ebisawa, K., Maeda, Y., Kaneda, H., & Yamauchi, S. 2001, *Science*, 293, 1633  
 Favata, F., Micela, G., & Sciortino, S. 1995, *A&A*, 298, 482  
 Feigelson, E. D. 2004, in *Stars As Suns: Activity, Evolution, and Planets*, A. Benz & A. Dupree (eds.) IAU Symposium 219, in press  
 Figer, D. F., Kim, S. S., Morris, M., Serabyn, E., Rich, R. M., & McLean, I. S. 1999, *ApJ*, 525, 750  
 Grosso, N., Montmerle, T., Feigelson, E. D., & Forbes, T. G. 2004, submitted to *A&A*  
 Ho, P. T. P., Jackson, J. M., Barret, A. H., & Armstrong, J. T. 1985, *ApJ*, 288, 575  
 Kaneda, H., Makishima, K., Yamauchi, S., Koyama, K., Matsuzaki, K., & Yamasaki, N. Y. 1997, *ApJ*, 491, 638  
 Killeen, N. E. B., Lo, K. Y., & Crutcher, R. 1992, *ApJ*, 385, 585  
 Krabbe, A. et al. 1995, *ApJ*, 447, L95  
 Koyama, K., Ikeuchi, S., & Tomisaka, K. 1986a, *PASJ*, 38, 503  
 Koyama, K., Maeda, Y., Sonobe, T., Takeshima, T., Tanaka, Y., & Yamauchi, S. 1996, *PASJ*, 48, 249  
 Koyama, K., Makishima, K., Tanaka, Y., & Tsunemi, H. 1986b, *PASJ*, 38, 121  
 LaRosa, T. N., Kassim, N. E., Lasio, T. J. W., & Hyman, S. D. 2000a, *AJ*, 119, 207  
 LaRosa, T. N., Lazio, T. J. W., & Kassim, N. E. 2001, *ApJ*, 563, 163  
 Launhardt, R., Zylka, R., & Mezger, P. G. 2002, *A&A*, 384, 112  
 Lebrun, F. et al. 2004, *Nature*, 428, 293  
 Leitherer, C., Robert, C., & Drissen, L. 1992, *ApJ*, 401, 596  
 Lu, F. J., Wang, Q. D., & Lang, C. C. 2003, *AJ*, 126, 319  
 Maeda, Y. et al. 2002, *ApJ*, 570, 671  
 Masai, K. 1984, *Ap&SS*, 98, 367  
 Masai, K., Dogiel, V. A., Inoue, H., Schönfelder, V., & Strong, A. W., 2002, *ApJ*, 581, 1071  
 Markevitch, M. et al. 2003, *ApJ*, 583, 70  
 McNamara, D. H., Madsen, J. B., Barnes, J., & Ericksen, B. F. 2000, *PASP*, 112, 202  
 Mewe, R., Lemen, J. R., & van den Oord, G. H. J. 1986, *A&AS*, 65, 511  
 Mezger, P. G., Duschl, W. J., & Zylka, R., 1996, *AARev*, 7, 289

- Morris, M., Baganoff, F., Muno, M., Howard, C., Maeda, Y., Feigelson, E., Bautz, M., Brandt, W. N., Chartas, G., Garmire, G., & Townsley, L. 2003, *Astronomische Nachrichten*, 324, S1, 167
- Muno, M. P., Baganoff, F. K., Bautz, M. W., Brandt, W. N., Broos, P. S., Feigelson, E. D., Garmire, G. P., Morris, M., Ricker, G. R., & Townsley, L. K. 2003a, *ApJ*, 589, 225
- Muno, M. P., Baganoff, F. K., & Arabdjis, J. S. 2003b, *ApJ*, 598, 474
- Muno, M. P., Baganoff, F. K., Bautz, M. W., Brandt, W. N., Feigelson, E. D., Garmire, G. P., Morris, M., & Ricker, G. R., in preparation for *ApJ*
- Murakami, H., Koyama, K., Sakano, M., & Tsujimoto, M. 2000, *ApJ*, 534, 283
- Novak, G. Chuss, D. T., Renebarger, T., Griffin, G. S., Newcomb, M. G., Peterson, J. B., Loewenstein, R. F., Pernic, D., & Dotson, J. L. 2003, *ApJ*, 583, L83
- Park, S., Baganoff, F. K., Morris, M., Maeda, Y., Muno, M. P., Howard, C., Bautz, M. W., & Garmire, G. P. 2004, *ApJ*, 603, 548
- Paumard, T., Maillard, J. P., Morris, M., & Rigaut, F. 2001, *A&A*, 366, 466
- Perna, R., Narayan, R., Rybicki, G., Stella, L., & Treves, A. 2003, *ApJ*, 594, 936
- Raymond, J. C. & Smith, B. W. 1977, *ApJS*, 35, 419
- Raymond, J. C., Cox, D. P., & Smith, B. W. 1976, *ApJ*, 204, 290
- Rosati, P. et al. 2002, *ApJ*, 566, 667
- Steward, F. D. & Chlebowski, T. 1982, *ApJ*, 256, 530
- Sakano, M., Warwick, R. S., Decourchelle, A., & Predehl, P. 2003, *MNRAS*, 340, 747
- Schwope, A. D., Brunner, H., Buckley, D., Greiner, J., Heyden, K. v. d., Neizvestny, S., Potter, S., & Schwarz, R. 2002, *A&A*, 396, 895
- Serabyn, E., & Morris, M. 1996, *ARA&A*, 34, 645
- Sidoli, L. & Mereghetti, S. 1999, *A&A*, 349, L49
- Singh, K. P., Drake, S. A., & White, N. E. 1996, *AJ*, 111, 2415
- Skibo, J. G., Johnson, W. N., Kurfess, J. D., Kinzer, R. L., Jung, G., Grove, J. E., Purcell, W. R., Ulmer, M. P., Gehrels, N., & Tueller, J. 1997, *ApJ*, 483, L95
- Schlickeiser, R. 2002, "Cosmic Ray Astrophysics", Springer-Verlag, Berlin
- Stevens, I. R., & Hartwell, J. M. 2003, *MNRAS*, 339, 280
- Sunyaev, R., Markevitch, M., & Pavlinsky, M. 1993, *ApJ*, 407, 606
- Tan, J. D. & Draine, B. T. 2003, *astro-ph/0310442*
- Tanaka, Y., Miyaji, T., & Hasinger, G. 1999, *Astron. Nachr.*, 320, 181
- Tanaka, Y., Koyama, K., Maeda, Y., & Sonobe, T. 2000, *PASJ*, 52, L25
- Tanaka, Y. 2002, *A&A*, 382, 1052
- Tanuma, S., Yokoyama, T., Kudoh, T., Matsumoto, R., Shibata, K., & Makishima, K. 1999, *PASJ*, 51, 161
- Townsley, L. K. et al., 2002a, *NIM-A*, 486, 716
- Townsley, L. K. et al., 2002b, *NIM-A*, 486, 751
- Townsley, L. K., Feigelson, E. D., Montmerle, T., Broos, P. S., Chu, Y.-H., & Garmire, G. P. 2003, *ApJ*, 593, 874
- Tsuboi, M., Handa, T., & Ukita, N. 1999, *ApJS*, 120, 1
- Uchida, K. I. & Güsten 1995, *A&A*, 298, 473
- Valinia, A. & Marshall, F. E. 1998, *ApJ*, 505, 134
- Valinia, A., Tatischeff, V., Arnaud, K., Ebisawa, K., & Ramaty, R. 2000, *ApJ*, 543, 733
- Vollmer, B., Zylka, R., & Duschl, W. J. 2003, *A&A* submitted, *astro-ph/0306200*
- Wang, Q. D., Gotthelf, E. V., & Lang, C. C. 2002, *Nature*, 415, 148
- Warner, B. 1995, *Cataclysmic Variable Stars*, Cambridge University Press
- Weisskopf, M. C., Brinkman, B., Canizares, C., Garmire, G., Murray, S., & van Speybroeck, L. P. 2002, *PASP*, 114, 1
- Worrall, D. M., Marshall, F. E., Boldt, E. A., & Swank, J. H. 1982, *ApJ*, 255, 111
- Yamauchi, S., Kaneda, H., Koyama, K., Makishima, K., Matsuzaki, K., Sonobe, T., Tanaka, Y., & Yamasaki, N. 1996, *PASJ*, 48, L15
- Yamauchi, S., Kawada, M., Koyama, K., Kunieda, H., Tawara, Y., & Hatsukade, I. 1990, *ApJ*, 365, 532
- Yamasaki, S. et al. 1997, *ApJ*, 481, 821
- Yusef-Zadeh, F. 2003, *astro-ph/0308008*
- Yusef-Zadeh, F. & Morris, M. 1987, *ApJ*, 322, 721
- Yusef-Zadeh, F., Law, C., & Wardle, M. 2002, *ApJ*, 568, L121
- Zane, S., Turolla, R., & Treves, A. 1996, *ApJ*, 471, 248
- Zylka, R., Mezger, P. G., & Wink, J. E. 1990, *A&A*, 234, 133

TABLE 1  
OBSERVATIONS OF THE INNER 20 PC OF THE GALAXY

Start Time (UT)	Sequence	Exposure (s)	Aim Point		Roll (degrees)
			RA (degrees J2000)	DEC	
1999 Sep 21 02:43:00	0242	40,872	266.41382	-29.0130	268
2000 Oct 26 18:15:11	1561	35,705	266.41344	-29.0128	265
2001 Jul 14 01:51:10	1561	13,504	266.41344	-29.0128	265
2002 Feb 19 14:27:32	2951	12,370	266.41867	-29.0033	91
2002 Mar 23 12:25:04	2952	11,859	266.41897	-29.0034	88
2002 Apr 19 10:39:01	2953	11,632	266.41923	-29.0034	85
2002 May 07 09:25:07	2954	12,455	266.41938	-29.0037	82
2002 May 22 22:59:15	2943	34,651	266.41991	-29.0041	76
2002 May 24 11:50:13	3663	37,959	266.41993	-29.0041	76
2002 May 25 15:16:03	3392	166,690	266.41992	-29.0041	76
2002 May 28 05:34:44	3393	158,026	266.41992	-29.0041	76
2002 Jun 03 01:24:37	3665	89,928	266.41992	-29.0041	76

TABLE 2  
EXTRACTION REGIONS FOR THE DIFFUSE EMISSION

Region	Area (arcmin <sup>2</sup> )	Offset (arcmin)	Net Counts	Background
Southeast	34.7	7.5	$1.44 \times 10^5$	$0.42 \times 10^5$
Southwest	14.0	7.7	$0.56 \times 10^5$	$0.17 \times 10^5$
Northwest	23.9	7.8	$0.82 \times 10^5$	$0.27 \times 10^5$
East	12.0	7.8	$0.65 \times 10^5$	$0.16 \times 10^5$
Close	9.0	3.9	$0.61 \times 10^5$	$0.12 \times 10^5$
Northeast	46.0	7.6	$4.74 \times 10^5$	$0.53 \times 10^5$

TABLE 3  
TWO- $kT$  PLASMA MODEL OF DIFFUSE EMISSION

	Southeast	Southwest	Northwest	East	Close	Northeast
$N_{H,s}$ ( $10^{22}$ cm <sup>-2</sup> )	$1.4^{+0.1}_{-0.1}$	$1.0^{+0.1}_{-0.2}$	$1.7^{+0.2}_{-0.2}$	$2.2^{+0.1}_{-0.2}$	$1.6^{+0.1}_{-0.2}$	$7.2^{+0.1}_{-0.1}$
$N_{H,pc,s}$ ( $10^{22}$ cm <sup>-2</sup> )	$4.8^{+0.3}_{-0.3}$	$4.4^{+1.0}_{-1.0}$	$4.9^{+0.6}_{-0.5}$	$4.7^{+0.4}_{-0.4}$	$4.8^{+0.7}_{-0.6}$	$0.1^{+11.2}_{-0.1}$
$f_s$ (fixed)	0.95	0.95	0.95	0.95	0.95	0.94
$kT_s$ (keV)	$0.82^{+0.03}_{-0.03}$	$0.71^{+0.05}_{-0.03}$	$0.70^{+0.03}_{-0.03}$	$0.92^{+0.08}_{-0.03}$	$0.80^{+0.07}_{-0.03}$	$0.88^{+0.02}_{-0.00}$
$K_{EM,s}$ ( $10^{-4}$ cm <sup>-6</sup> pc)	$2.1^{+0.2}_{-0.3}$	$1.3^{+0.3}_{-0.4}$	$2.2^{+0.6}_{-0.5}$	$5.9^{+1.2}_{-1.4}$	$3.0^{+0.8}_{-0.8}$	$22.0^{+1.1}_{-0.9}$
$F_s$ ( $10^{-13}$ erg cm <sup>-2</sup> s <sup>-1</sup> arcmin <sup>-2</sup> )	0.3	0.2	0.2	0.6	0.4	1.7
$uF_s$ ( $10^{-13}$ erg cm <sup>-2</sup> s <sup>-1</sup> arcmin <sup>-2</sup> )	0.8	0.4	0.7	2.1	1.1	5.6
$N_{H,h}$ ( $10^{22}$ cm <sup>-2</sup> )	$4.8^{+0.3}_{-0.2}$	$4.0^{+0.5}_{-0.3}$	$6.1^{+0.4}_{-0.4}$	$4.7^{+0.6}_{-0.3}$	$4.7^{+0.4}_{-0.3}$	$1.16^{+0.03}_{-0.04}$
$N_{H,pc,h}$ ( $10^{22}$ cm <sup>-2</sup> )	$83^{+25}_{-20}$	$29^{+13}_{-6}$	$72^{+24}_{-15}$	$70^{+40}_{-13}$	$28^{+9}_{-6}$	$14.7^{+1.3}_{-0.4}$
$f_h$	$0.50^{+0.14}_{-0.12}$	$0.52^{+0.05}_{-0.05}$	$0.60^{+0.11}_{-0.09}$	$0.58^{+0.19}_{-0.13}$	$0.48^{+0.05}_{-0.05}$	$0.95^{+0.04}_{-0.03}$
$kT_h$ (keV)	$7.1^{+0.7}_{-0.8}$	$8.1^{+0.6}_{-0.6}$	$8.8^{+0.7}_{-0.5}$	$5.9^{+0.7}_{-1.1}$	$8.6^{+0.7}_{-0.4}$	$7.9^{+0.3}_{-0.2}$
$K_{EM,h}$ ( $10^{-4}$ cm <sup>-6</sup> pc)	$1.8^{+0.6}_{-0.5}$	$1.5^{+0.3}_{-0.2}$	$2.2^{+0.8}_{-0.4}$	$2.5^{+1.8}_{-0.7}$	$2.2^{+0.3}_{-0.2}$	$2.7^{+0.0}_{-0.1}$
$F_h$ ( $10^{-13}$ erg cm <sup>-2</sup> s <sup>-1</sup> arcmin <sup>-2</sup> )	1.5	1.6	1.5	1.6	2.5	2.4
$uF_h$ ( $10^{-13}$ erg cm <sup>-2</sup> s <sup>-1</sup> arcmin <sup>-2</sup> )	4.0	3.5	5.1	5.9	5.3	5.6
$Z_{Si}/Z_{Si,\odot}$	$1.0^{+0.1}_{-0.1}$	$1.5^{+0.5}_{-0.3}$	$1.5^{+0.3}_{-0.2}$	$0.7^{+0.2}_{-0.1}$	$1.3^{+0.3}_{-0.3}$	$0.80^{+0.03}_{-0.04}$
$Z_S/Z_{S,\odot}$	$2.5^{+0.4}_{-0.2}$	$2.7^{+0.8}_{-0.6}$	$2.2^{+0.5}_{-0.3}$	$1.6^{+0.3}_{-0.3}$	$2.3^{+0.6}_{-0.5}$	$1.03^{+0.04}_{-0.01}$
$Z_{Ar}/Z_{Ar,\odot}$	$3.6^{+0.6}_{-0.4}$	$4.1^{+1.2}_{-1.1}$	$2.8^{+0.8}_{-0.6}$	$1.8^{+0.4}_{-0.4}$	$3.3^{+0.9}_{-0.8}$	$1.08^{+0.06}_{-0.05}$
$Z_{Ca}/Z_{Ca,\odot}$	$2.4^{+0.5}_{-0.5}$	$2.3^{+1.3}_{-1.1}$	$1.3^{+0.8}_{-0.8}$	$2.0^{+0.4}_{-0.5}$	$2.4^{+0.8}_{-0.8}$	$1.1^{+0.1}_{-0.1}$
$Z_{Fe}/Z_{Fe,\odot}$	$0.7^{+0.1}_{-0.2}$	$0.8^{+0.1}_{-0.1}$	$0.7^{+0.1}_{-0.1}$	$0.7^{+0.2}_{-0.2}$	$0.8^{+0.1}_{-0.1}$	$0.57^{+0.04}_{-0.02}$
Fe K- $\alpha$ ( $10^{-7}$ ph cm <sup>-2</sup> s <sup>-1</sup> arcmin <sup>-2</sup> )	$11^{+4}_{-2}$	$9^{+1}_{-1}$	$15^{+5}_{-2}$	$14^{+9}_{-3}$	$14^{+2}_{-1}$	$42^{+1}_{-1}$
$\chi^2/\nu$	494.0/462	484.4/462	519.1/462	621.8/462	428.5/462	519.9/462

Note. — The fluxes  $F$  and  $uF$  are between 2–8 keV. The former is the observed flux, the latter is the de-absorbed flux.

TABLE 4  
PROPERTIES OF IRON EMISSION

	Southeast	Southwest	Northwest	East	Close	Northeast
$\Gamma$	$1.1^{+0.1}_{-0.1}$	$0.5^{+0.2}_{-0.2}$	$0.5^{+0.1}_{-0.2}$	$1.1^{+0.2}_{-0.2}$	$0.8^{+0.1}_{-0.2}$	$1.4^{+0.0}_{-0.1}$
$N_\Gamma$ ( $10^{-5}$ ph cm <sup>-2</sup> s <sup>-1</sup> keV <sup>-1</sup> arcmin <sup>-2</sup> )	$1.9^{+0.4}_{-0.6}$	$0.7^{+0.3}_{-0.2}$	$0.7^{+0.2}_{-0.2}$	$2.2^{+0.9}_{-0.7}$	$2.1^{+0.5}_{-0.5}$	$7.3^{+0.6}_{-0.6}$
$E_{FeK-\alpha}$ (keV)	$6.39^{+0.01}_{-0.01}$	$6.37^{+0.03}_{-0.03}$	$6.443^{+0.011}_{-0.008}$	$6.38^{+0.04}_{-0.04}$	$6.40^{+0.01}_{-0.02}$	$6.395^{+0.002}_{-0.002}$
$W_{FeK-\alpha}$ (eV) <sup>a</sup>	< 70	40	40	40	40	$37^{+9}_{-10}$
$I_{FeK-\alpha}$ ( $10^{-7}$ ph cm <sup>-2</sup> s <sup>-1</sup> arcmin <sup>-2</sup> )	$4.0^{+0.5}_{-0.4}$	$3.9^{+0.8}_{-0.8}$	$7.6^{+0.9}_{-0.5}$	$5.9^{+1.0}_{-1.3}$	$8.4^{+1.0}_{-0.8}$	$30.9^{+0.5}_{-0.5}$
$E_{FeHe-\alpha}$ (keV)	$6.637^{+0.006}_{-0.008}$	$6.665^{+0.009}_{-0.020}$	$6.73^{+0.01}_{-0.02}$	$6.670^{+0.02}_{-0.02}$	$6.658^{+0.007}_{-0.017}$	$6.668^{+0.004}_{-0.005}$
$W_{FeHe-\alpha}$ (eV) <sup>a</sup>	< 40	40	40	40	40	$50^{+15}_{-30}$
$I_{FeHe-\alpha}$ ( $10^{-7}$ ph cm <sup>-2</sup> s <sup>-1</sup> arcmin <sup>-2</sup> )	$12.2^{+0.5}_{-0.7}$	$12^{+1}_{-1}$	$10.3^{+0.7}_{-1.5}$	$16^{+1}_{-2}$	$17^{+1}_{-2}$	$16.8^{+0.6}_{-0.6}$
$E_{FeH-\alpha}$ (keV)	$6.86^{+0.05}_{-0.05}$	$6.98^{+0.03}_{-0.08}$	$6.94^{+0.03}_{-0.04}$	$6.97^b$	$6.94^{+0.01}_{-0.04}$	$6.948^{+0.006}_{-0.007}$
$W_{FeH-\alpha}$ (eV)	0	0	0	0	0	0
$I_{FeH-\alpha}$ ( $10^{-7}$ ph cm <sup>-2</sup> s <sup>-1</sup> arcmin <sup>-2</sup> )	$2.8^{+1.0}_{-0.4}$	$4.7^{+1.2}_{-1.4}$	$4.2^{+0.5}_{-1.3}$	< 2.7	$8.2^{+1.5}_{-1.5}$	$6.7^{+0.7}_{-0.7}$
$I_{K-\alpha}/I_{He-\alpha}$	$0.3^{+0.1}_{-0.0}$	$0.3^{+0.1}_{-0.1}$	$0.7^{+0.2}_{-0.1}$	$0.4^{+0.1}_{-0.1}$	$0.5^{+0.1}_{-0.1}$	$1.8^{+0.1}_{-0.1}$
$I_{He-\alpha}/I_{H-\alpha}$	$4.4^{+1.2}_{-1.6}$	$2.5^{+1.8}_{-0.8}$	$2.5^{+1.4}_{-0.5}$	> 4.3	$2.1^{+0.7}_{-0.5}$	$2.5^{+0.5}_{-0.3}$
$\chi^2/\nu$	204.1/230	245.6/230	236.8/230	315.0/231	219.9/230	240.6/230

<sup>a</sup>The widths of the K- $\alpha$  and He- $\alpha$  lines were only allowed to vary for the spectra from the Northeast and Southeast.

<sup>b</sup>The H- $\alpha$  line was not detected in the East, so its centroid was fixed in order to obtain an upper limit to the line flux.

TABLE 5  
FLUX FROM THE PLASMA COMPONENTS AND POINT SOURCES

	Southeast	Southwest	Northwest	East	Close	Northeast
	Total Fluxes from Regions					
$F_{\text{tot}}$	1.8	1.8	1.7	2.3	3.0	4.5
$F_{\text{detected}}$	0.2	0.3	0.2	0.2	1.0	0.4
Component Fluxes Assuming No Undetected Point Source Component						
$F_{\text{s}}$	0.3	0.2	0.2	0.6	0.4	1.8
$F_{\text{h}}$	1.5	1.6	1.5	1.6	2.5	2.6
Component Fluxes with Undetected Point Source Component						
$F_{\text{s}}$	0.5	0.4	0.2	0.5	0.5	1.7
$F_{\text{h}}$	0.0	0.0	0.8	0.9	0.1	1.9
$F_{\text{undetected}}$	1.3	1.4	0.7	0.8	2.4	0.9

Note. —  $F_{\text{tot}}$  denotes the total diffuse flux,  $F_{\text{detected}}$  the total flux from detected point sources,  $F_{\text{s}}$  the soft component of the diffuse flux,  $F_{\text{h}}$  the hard component, and  $F_{\text{undetected}}$  the maximum contribution from undetected point sources. All fluxes are those observed between 2–8 keV, in units of  $10^{-13}$  erg  $\text{cm}^{-2}$   $\text{s}^{-1}$   $\text{arcmin}^{-2}$ .

TABLE 6  
PROPERTIES OF THE PLASMA COMPONENTS

	Scaling	Southeast	Southwest	Northwest	East	Close	Northeast
Soft Component							
$L_X$ ( $10^{33}$ erg $\text{s}^{-1}$ $\text{arcmin}^{-2}$ )		11.8	6.3	10.1	32.8	16.4	87.1
$kT$ (keV)		0.8	0.7	0.7	0.9	0.8	0.9
$n$ ( $\text{cm}^{-3}$ )	$d_{50}^{-1/2}$	0.1	0.1	0.2	0.2	0.2	0.5
$M$ ( $M_{\odot}$ $\text{arcmin}^{-2}$ )	$d_{50}^{1/2}$	1.0	0.8	1.0	1.6	1.2	3.1
$U$ ( $10^{-9}$ erg $\text{cm}^{-3}$ )	$d_{50}^{-1/2}$	0.3	0.2	0.3	0.5	0.3	1.0
$E$ ( $10^{48}$ erg $\text{arcmin}^{-2}$ )	$d_{50}^{1/2}$	2	2	2	4	3	8
$t_{\text{cool}}$ ( $10^7$ yr)	$d_{50}^{3/2}$	0.6	0.8	0.6	0.4	0.5	0.3
$c_s$ ( $\text{km s}^{-1}$ )		510	470	470	540	500	530
$t_{\text{exp}}$ ( $10^5$ yr)	$d_{50}$	0.9	1.0	1.0	0.9	1.0	0.9
$\dot{W}$ ( $10^{36}$ erg $\text{s}^{-1}$ )	$d_{50}^{1/6}$	4	2	3	8	4	14
$t_{PdV}$ ( $10^4$ yr)	$d_{50}^{1/3}$	2	2	2	2	2	2
Hard Component							
$L_X$ ( $10^{33}$ erg $\text{s}^{-1}$ $\text{arcmin}^{-2}$ )		6.2	5.4	7.9	9.1	8.2	8.7
$kT$ (keV)		7.1	8.1	8.8	5.9	8.6	7.9
$n$ ( $\text{cm}^{-3}$ )	$d_{50}^{-1/2}$	0.1	0.1	0.2	0.2	0.2	0.2
$M$ ( $M_{\odot}$ $\text{arcmin}^{-2}$ )	$d_{50}^{1/2}$	0.9	0.8	1.0	1.1	1.0	1.1
$U$ ( $10^{-9}$ erg $\text{cm}^{-3}$ )	$d_{50}^{-1/2}$	2	2	3	2	3	3
$E$ ( $10^{48}$ erg $\text{arcmin}^{-2}$ )	$d_{50}^{1/2}$	18	19	24	18	24	25
$t_{\text{cool}}$ ( $10^7$ yr)	$d_{50}^{3/2}$	10	11	10	6	10	9
$c_s$ ( $\text{km s}^{-1}$ )		1500	1600	1700	1400	1600	1600
$t_{\text{exp}}$ ( $10^5$ yr)	$d_{50}$	0.3	0.3	0.3	0.4	0.3	0.3
$\dot{W}$ ( $10^{36}$ erg $\text{s}^{-1}$ )	$d_{50}^{1/6}$	90	100	136	80	134	130
$t_{PdV}$ ( $10^4$ yr)	$d_{50}^{1/3}$	0.6	0.6	0.6	0.7	0.6	0.6

TABLE 7  
SUMMARY OF X-RAYS FROM THE GALACTIC CENTER

Source	Size (arcmin <sup>2</sup> )	$L_X$ (erg s <sup>-1</sup> ; 2–8 keV)	References
Sgr A*	$7 \times 10^{-5}$	$2 \times 10^{33}$	[1]
Central Stellar Cluster	0.08	$2 \times 10^{33}$	[1]
Sgr A East	1.4	$8 \times 10^{34}$	[2]
Bipolar Outflow	30	$2 \times 10^{34}$	[3]
Non-thermal Filaments	0.04	$1 \times 10^{34}$	[4]
Neutral Iron Filaments	0.5	$2 \times 10^{34}$	[5]
Detected Point Sources	290	$1 \times 10^{35}$	[6]
Diffuse Emission	290	$2 \times 10^{36}$	[7]

References. — [1] Baganoff et al. (2003); [2] Maeda et al. (2002); [3] Morris et al. (2003) [4] F. Yusef-Zadeh et al., in preparation; [5] Park et al. (2004); [6] Munro et al. (2003a); [7] this work